

## Electronic Supplementary Information to

### **New chiral ECD-Raman spectroscopy of atropisomeric naphthalenediimides**

Ewa Machalska,<sup>a,b</sup> Grzegorz Zając,<sup>\*b,c</sup> Malgorzata Baranska,<sup>a,b</sup> Petr Bouř,<sup>\*c</sup> Dorota Kaczorek,<sup>d</sup> Robert Kawęcki,<sup>\*d</sup>  
Joanna E. Rode,<sup>e</sup> Krzysztof Lyczko,<sup>e</sup> Jan Cz. Dobrowolski<sup>\*e</sup>

<sup>a</sup> Faculty of Chemistry, Jagiellonian University, Gronostajowa 2, 30-387 Cracow (Poland)

<sup>b</sup> Jagiellonian Centre for Experimental Therapeutics (JCET), Jagiellonian University, Bobrzyńskiego 14, 30-348 Cracow (Poland), E-mail: grzesiek.zajac@uj.edu.pl

<sup>c</sup> Institute of Organic Chemistry and Biochemistry, Academy of Sciences, Flemingovo náměstí 2, 16610, Prague, (Czech Republic), E-mail: bour@uochb.cas.cz

<sup>d</sup> Faculty of Science, Siedlce University, 3 Maja Street No 54, 08-110 Siedlce (Poland), E-mail: rkaw@uph.edu.pl

<sup>e</sup> Laboratory for Spectroscopy, Molecular Modeling and Structure Determination, Institute of Nuclear Chemistry and Technology, 16 Dorodna-Street, 03-195 Warsaw (Poland), E-mail: j.dobrowolski@nil.gov.pl

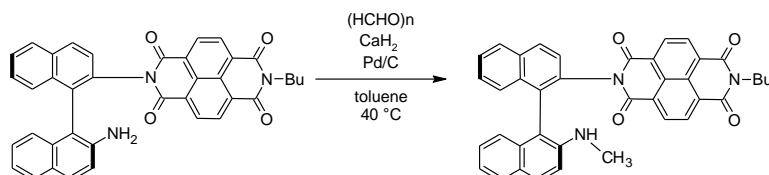
**Table of Contents**

<b>1. Synthesis</b> .....	3
(S)-NDIB-NHMe.....	3
(S)-NDIB-OH.....	4
(S)-NDIB-OMe.....	6
(S)-NDIB-NO <sub>2</sub> .....	7
<b>2. X-ray crystallography</b> .....	9
<b>3. DFT calculations of the substituent effect</b> .....	15
<b>4. ECD measurements</b> .....	23
<b>5. Explanation of the first ECD band sign by the DFT calculations</b> .....	26
<b>6. The Raman and ROA measurements</b> .....	31
<b>7. Simulation of the Raman, ROA and ECD-Raman spectra</b> .....	33

## 1. Synthesis

All commercially obtained reagents were used as received, unless otherwise stated. Column chromatography was performed using Acros Organics 60 Å silica gel (flash grade) with the indicated solvents. Nuclear magnetic resonance spectra were recorded on a 400 MHz instrument and were referenced to residual solvent signals (chloroform  $\delta = 7.26$  and 77.0 ppm for  $^1\text{H}$  NMR and  $^{13}\text{C}$  NMR, respectively). High-resolution mass spectra (HRMS) were obtained using an electrospray ionization source. *N*-Butyl-1,4,5,8-naphthalenetetracarboxylic-1,8-anhydride-4,5-imide and *N*-[2'-amino-(1,1'-binaphthalen-2-yl)]-*N*-butyl-naphthalene-1,4,5,8-tetracarboxylic acid bisimide (**NDIB-NH<sub>2</sub>**) were prepared as described in Ref. 1.<sup>1</sup>

### (*S*)-*N*-[2'-Methylamino-(1,1'-binaphthalen-2-yl)]-*N*-butyl-naphthalene-1,4,5,8-tetracarboxylic acid bisimide (*S*)-NDIB-NHMe

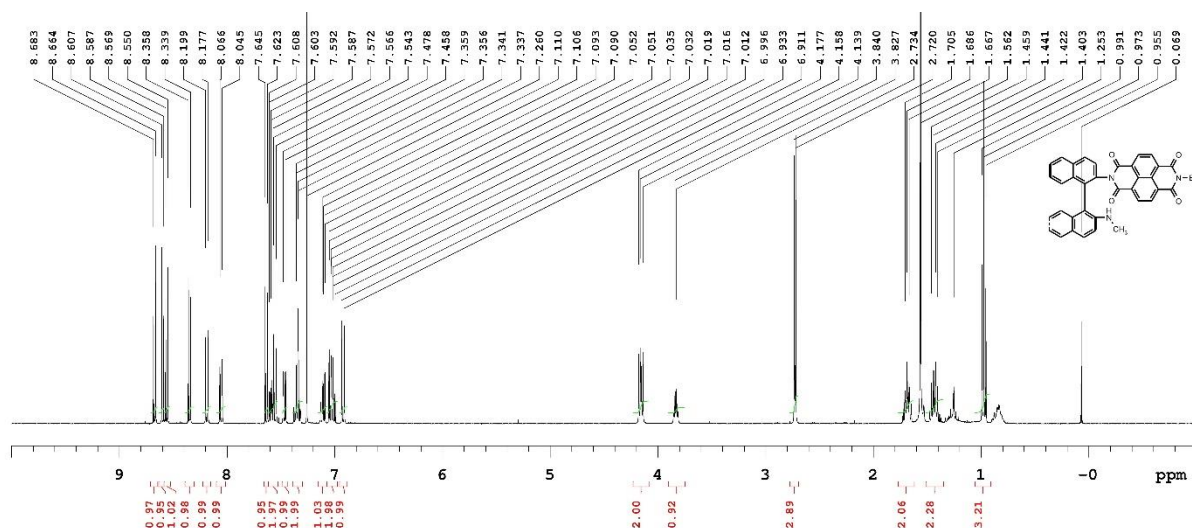


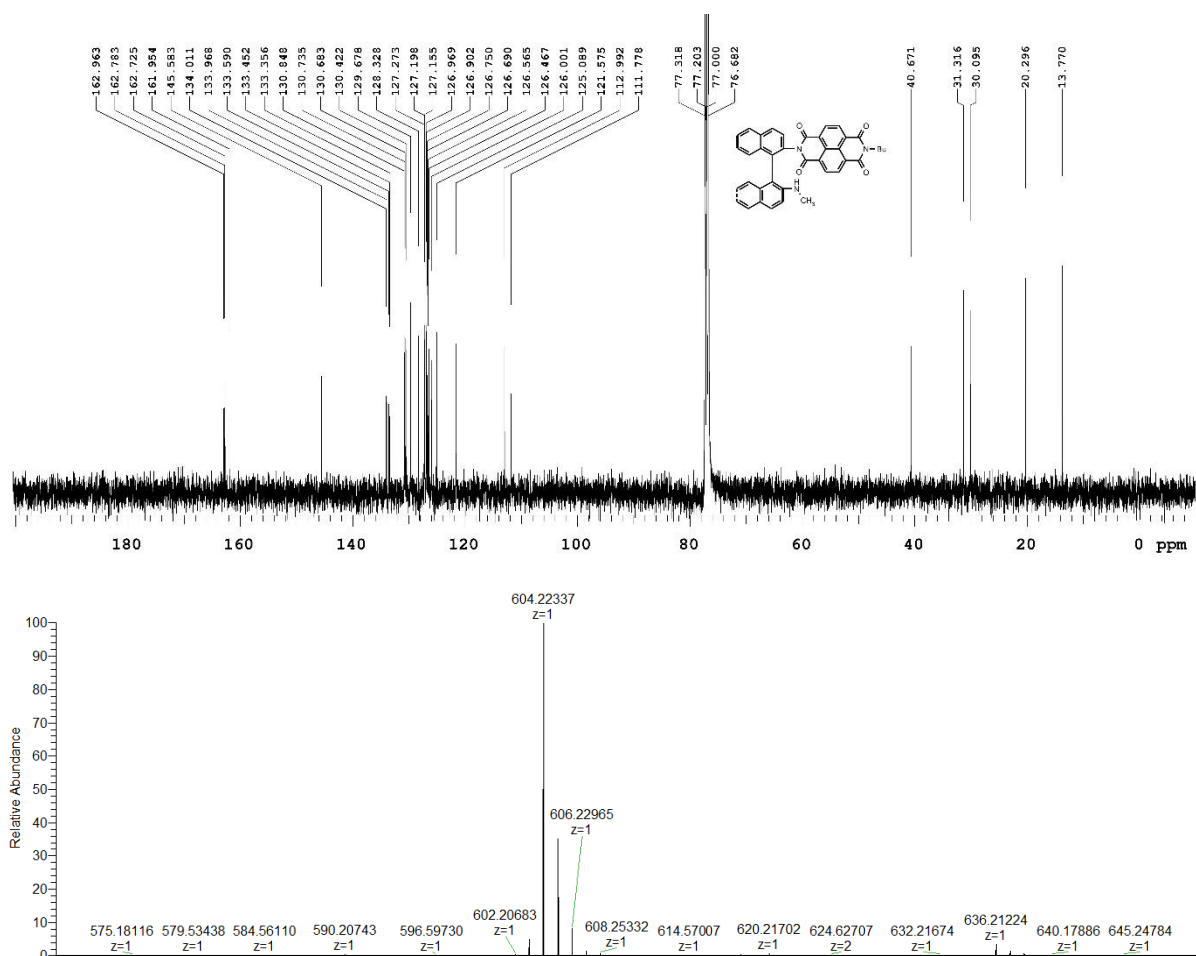
Monomethylation was performed using the modified procedure described by Guyon et al.<sup>2</sup> To a solution of (**S**)-NDIB-NH<sub>2</sub> (86 mg, 0.146 mmol) in toluene (3 mL), paraformaldehyde (7 mg, 0.219 mmol), Pd/C (10%, 5 mg) and CaH<sub>2</sub> (20 mg, 0.489 mmol) was added. The mixture was stirred under argon for 4 days at 40 °C. New portions of paraformaldehyde (7 mg, 0.219 mmol) and CaH<sub>2</sub> (20 mg, 0.489 mmol) were added every day. The reaction mixture was centrifuged. The supernatant was evaporated and the residue was purified by silica gel chromatography (CH<sub>2</sub>Cl<sub>2</sub>) to give 46 mg (52 %) solid.

$^1\text{H}$  NMR (400MHz, CDCl<sub>3</sub>)  $\delta$  = 8.67 (d, *J* = 7.7 Hz, 1 H), 8.60 (d, *J* = 7.7 Hz, 1 H), 8.56 (d, *J* = 7.7 Hz, 1 H), 8.35 (d, *J* = 7.7 Hz, 1 H), 8.19 (d, *J* = 8.7 Hz, 1 H), 8.06 (d, *J* = 8.1 Hz, 1 H), 7.63 (d, *J* = 8.7 Hz, 1 H), 7.59 (ddd, *J* = 1.9, 6.2, 8.1 Hz, 1 H), 7.55 (d, *J* = 9.3 Hz, 1 H), 7.47 (d, *J* = 7.9 Hz, 1 H), 7.39-7.30 (m, 2 H), 7.14 - 7.08 (m, 1 H), 7.07 - 7.03 (m, 1 H), 7.03 - 6.98 (m, 1 H), 6.92 (d, *J* = 9.1 Hz, 1 H), 4.19-4.12 (m, 2 H), 3.83 (q, *J* = 5.4 Hz, 1 H), 2.73 (d, *J* = 5.4 Hz, 3 H), 1.74 - 1.63 (m, 2 H), 1.43 (sex, *J* = 7.4 Hz, 2 H), 0.97 (t, *J* = 7.4 Hz, 3 H).

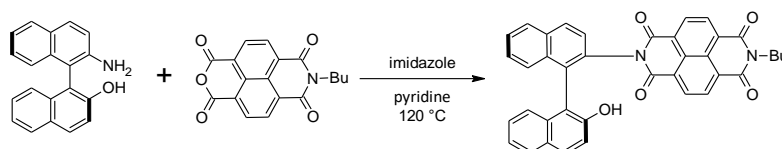
$^{13}\text{C}$  NMR (100MHz, CDCl<sub>3</sub>)  $\delta$  = 163.0, 162.8, 162.7, 161.9, 145.6, 134.4, 134.0, 133.96, 133.6, 133.4, 133.35, 130.84, 130.72, 130.67, 130.4, 129.67, 129.65, 128.3, 127.3, 127.18, 127.14, 127.0, 126.9, 126.74, 126.68, 126.6, 126.47, 126.45, 126.44, 126.0, 125.1, 121.6, 113.0, 111.8, 40.7, 31.3, 30.1, 20.3, 13.8.

HRMS (ESI) *m/z* calcd for C<sub>39</sub>H<sub>30</sub>N<sub>3</sub>O<sub>4</sub> (M+H)<sup>+</sup> 604.2231. Found: 604.2234.





**(S)-N-[2'-Hydroxy-(1,1'-binaphthalen-2-yl)]-N-butyl-naphthalene-1,4,5,8-tetracarboxylic acid bisimide (S)-NDIB-OH**

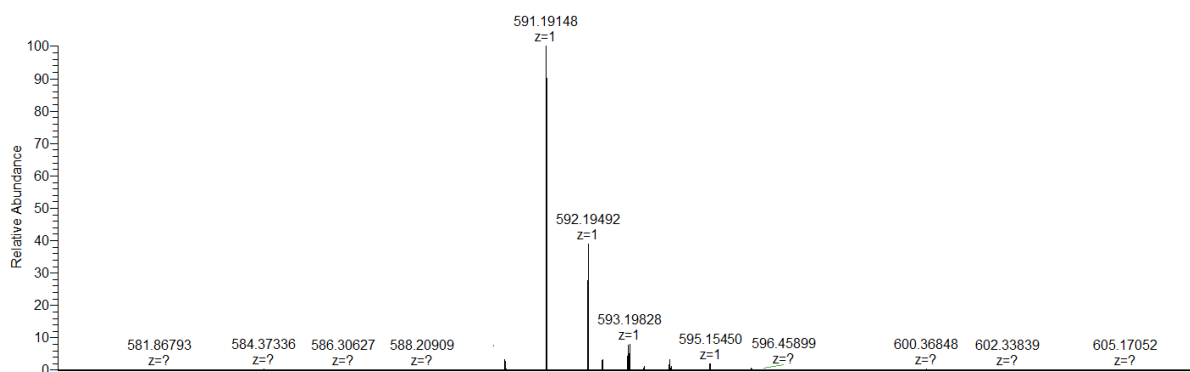
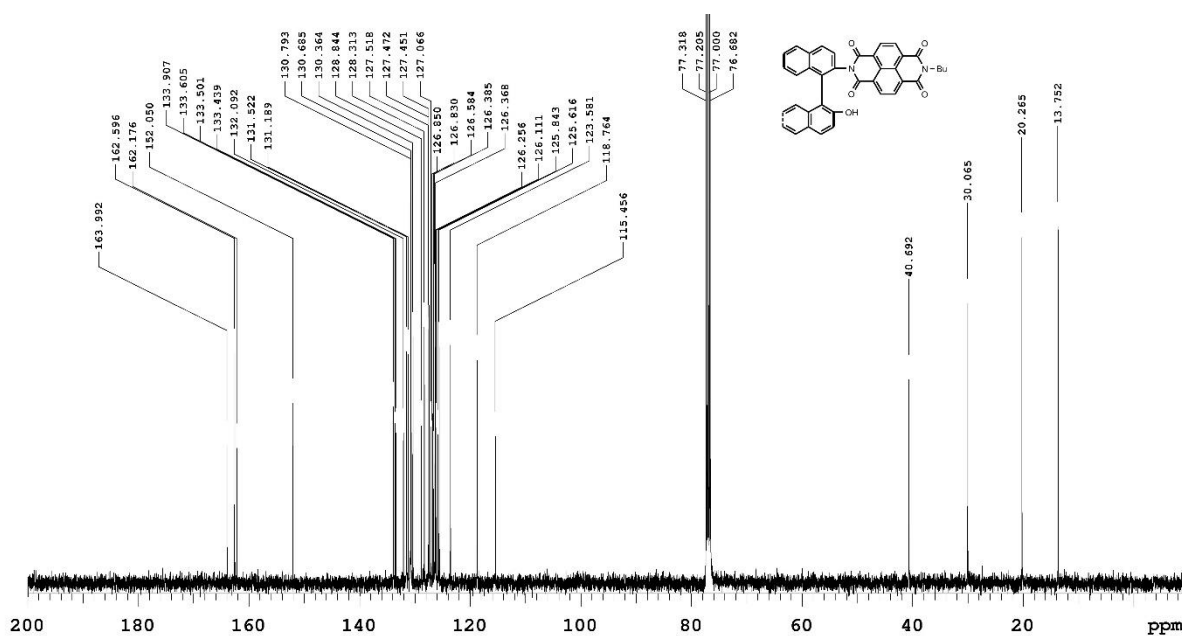
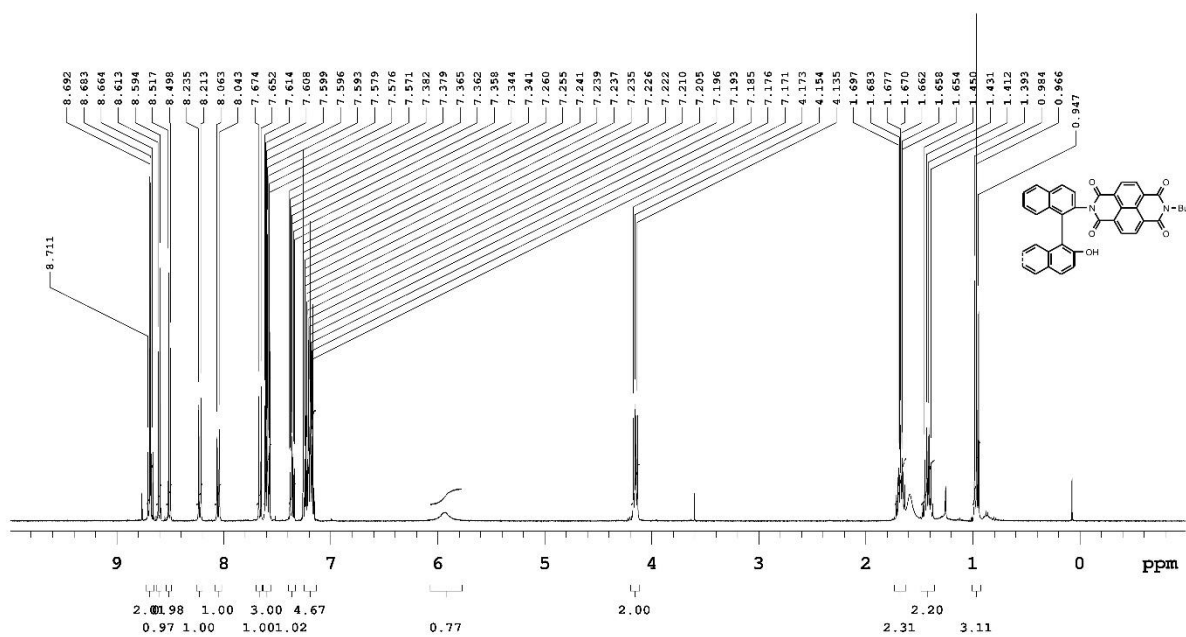


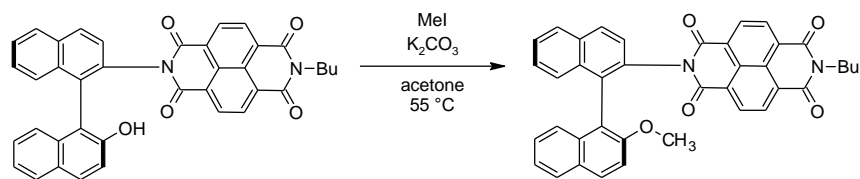
N-Butyl-1,4,5,8-naphthalenetetracarboxylic-1,8-anhydride-4,5-imide (320 mg, 0.987 mmol), NOBIN (255 mg, 0.898 mmol) and imidazole (320 mg, 4.669 mmol) were stirred in pyridine (10 mL) at 120°C for 24 h under argon. After cooling the reaction mixture was acidified with 10% aq HCl. The obtained precipitate was centrifuged and washed three times with water. The precipitate was dissolved in CH<sub>2</sub>Cl<sub>2</sub>, dried over MgSO<sub>4</sub>, filtered, and concentrated under reduced pressure. The product was purified by chromatography on silica gel in CH<sub>2</sub>Cl<sub>2</sub>-methanol (100:1, v / v) to give 401 mg (50%) of beige solid.

<sup>1</sup>H NMR (400MHz, CDCl<sub>3</sub>) δ = 8.70 (1/2AB, J = 7.7 Hz, 1 H), 8.68 (1/2AB, J = 7.7 Hz, 1 H), 8.60 (d, J = 7.7 Hz, 1 H), 8.51 (d, J = 7.7 Hz, 1 H), 8.22 (d, J = 8.7 Hz, 1 H), 8.05 (d, J = 8.3 Hz, 1 H), 7.66 (d, J = 8.7 Hz, 1 H), 7.62 - 7.56 (m, 3 H), 7.36 (ddd, J = 1.2, 6.9, 8.4 Hz, 1 H), 7.26 - 7.15 (m, 5 H), 5.94 (br, 1H), 4.18 - 4.12 (m, 2 H), 1.72 - 1.63 (m, 2 H), 1.42 (sex, J = 7.5, Hz, 2 H), 0.97 (t, J = 7.5 Hz, 3 H).

<sup>13</sup>C NMR (100MHz, CDCl<sub>3</sub>) δ = 164.0, 162.59, 162.58, 162.2, 152.0, 133.9, 133.6, 133.5, 133.4, 132.1, 131.5, 131.2, 130.79, 130.78, 130.7, 130.4, 128.8, 128.3, 127.51, 127.47, 127.44, 127.1, 126.84, 126.82, 126.6, 126.38, 126.36, 126.3, 126.1, 125.8, 125.6, 123.6, 118.8, 115.4, 40.7, 30.1, 20.3, 13.8.

HRMS (ESI) m/z calcd for C<sub>38</sub>H<sub>27</sub>N<sub>2</sub>O<sub>5</sub> (M+H)<sup>+</sup> 591.1915. Found: 591.1915.



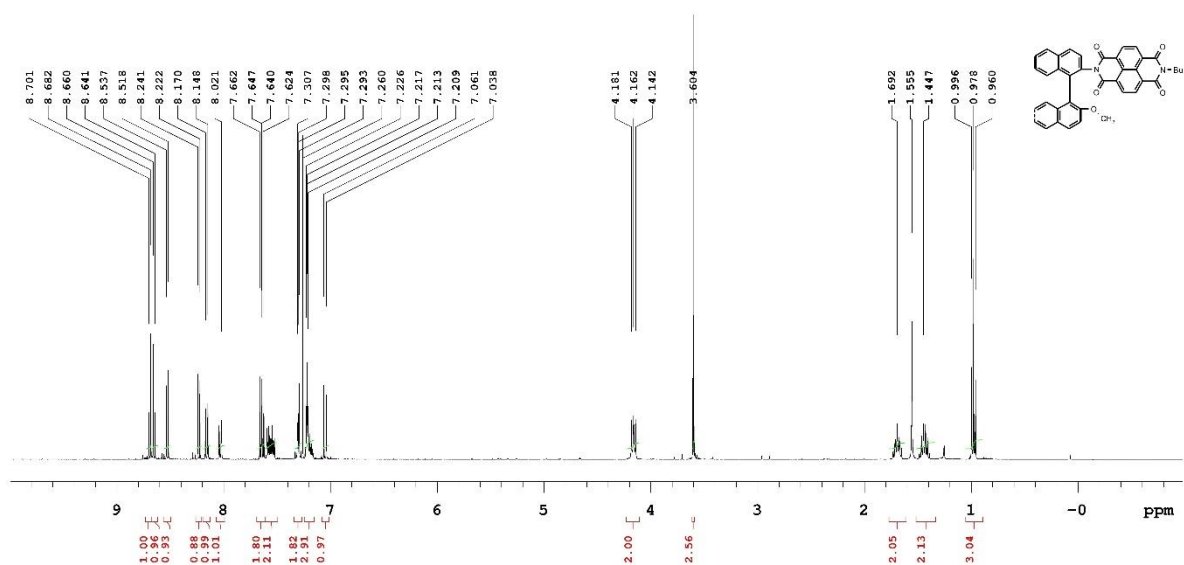
**(S)-N-[2'-Methoxy-(1,1'-binaphthalen-2-yl)]-N-butyl-naphthalene-1,4,5,8-tetracarboxylic acid bisimide (S)-NDIB-OMe**

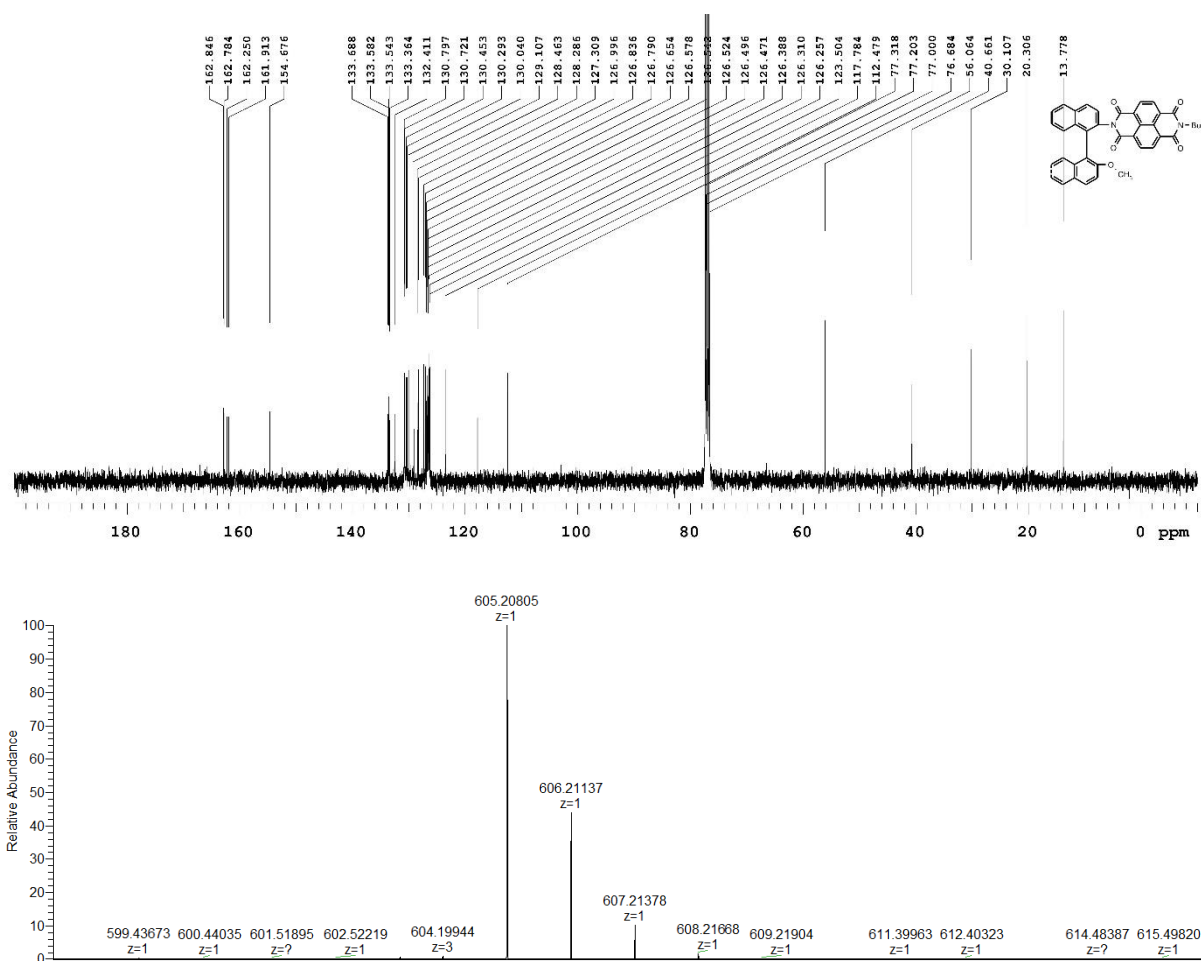
To a solution of **(S)-NDIB-OH** (50 mg, 0.084 mmol) in acetone (3 mL) was added iodomethane (59 mg, 0.422 mmol) and  $K_2CO_3$  (17 mg, 0.126 mmol). The mixture was stirred under argon for 3 h at 55°C (reflux). The progress of the reaction was followed by NMR. After completion of the reaction, the solution was evaporated, dissolved in  $CH_2Cl_2$ , filtered, and evaporated again. The residue was purified by chromatography on silica gel using  $CH_2Cl_2$ -methanol (first 300:1 then 150:1 v/v) to give solid 47 mg (92%).

$^1H$  NMR (400MHz,  $CDCl_3$ )  $\delta$  = 8.69 (d,  $J$  = 7.5 Hz, 1 H), 8.65 (d,  $J$  = 7.5 Hz, 1 H), 8.53 (d,  $J$  = 7.7 Hz, 1 H), 8.23 (d,  $J$  = 7.7 Hz, 1 H), 8.16 (d,  $J$  = 8.7 Hz, 1 H), 8.03 (d,  $J$  = 8.3 Hz, 1 H), 7.65 (d,  $J$  = 8.7 Hz, 1 H), 7.64 (d,  $J$  = 7.7 Hz, 1 H), 7.61 - 7.51 (m, 2 H), 7.34 - 7.27 (m, 2 H), 7.24 - 7.16 (m, 3 H), 7.05 (d,  $J$  = 9.1 Hz, 1 H), 4.19 - 4.13 (m, 2 H), 3.60 (s, 3 H), 1.74 - 1.64 (m, 2 H), 1.44 (sex,  $J$  = 7.5 Hz, 2 H), 0.98 (t,  $J$  = 7.5 Hz, 3 H).

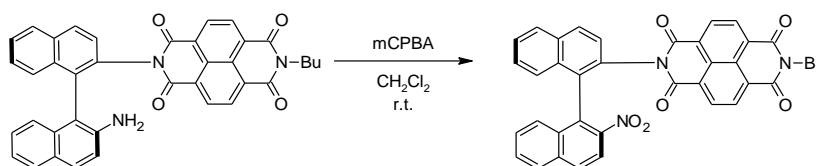
$^{13}C$  NMR (100MHz,  $CDCl_3$ )  $\delta$  = 162.84, 162.77, 162.2, 161.9, 154.7, 133.7, 133.6, 133.5, 133.4, 132.4, 130.8, 130.7, 130.4, 130.3, 130.0, 129.1, 128.5, 128.3, 127.3, 127.0, 126.83, 126.78, 126.65, 126.57, 126.54, 126.52, 126.49, 126.46, 126.38, 126.30, 126.25, 123.5, 117.8, 112.5, 56.1, 40.7, 30.1, 20.3, 13.8.

HRMS (ESI)  $m/z$  calcd for  $C_{39}H_{29}N_2O_5$  ( $M+H$ ) $^+$  605.2071. Found: 605.2081.





**(S)-N-[2'-Nitro-(1,1'-binaphthalen-2-yl)]-N-butyl-naphthalene-1,4,5,8-tetracarboxylic acid bisimide (S)-NDIB-NO<sub>2</sub>**

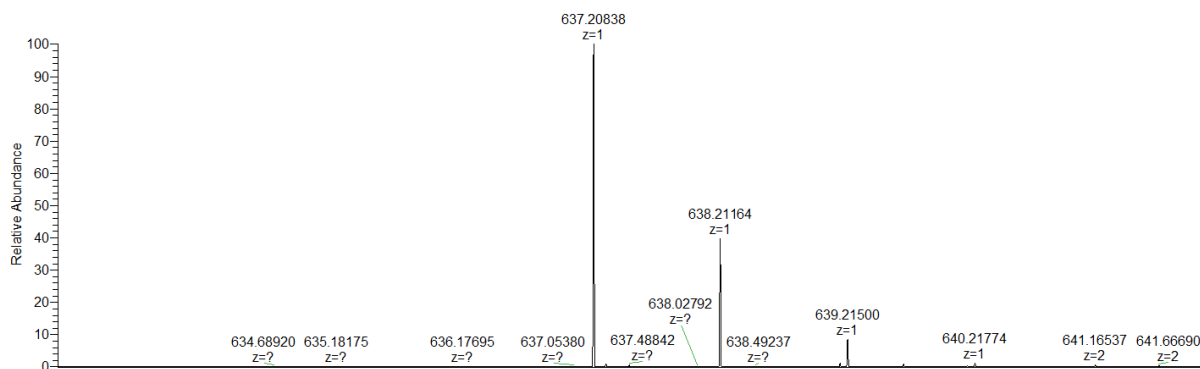
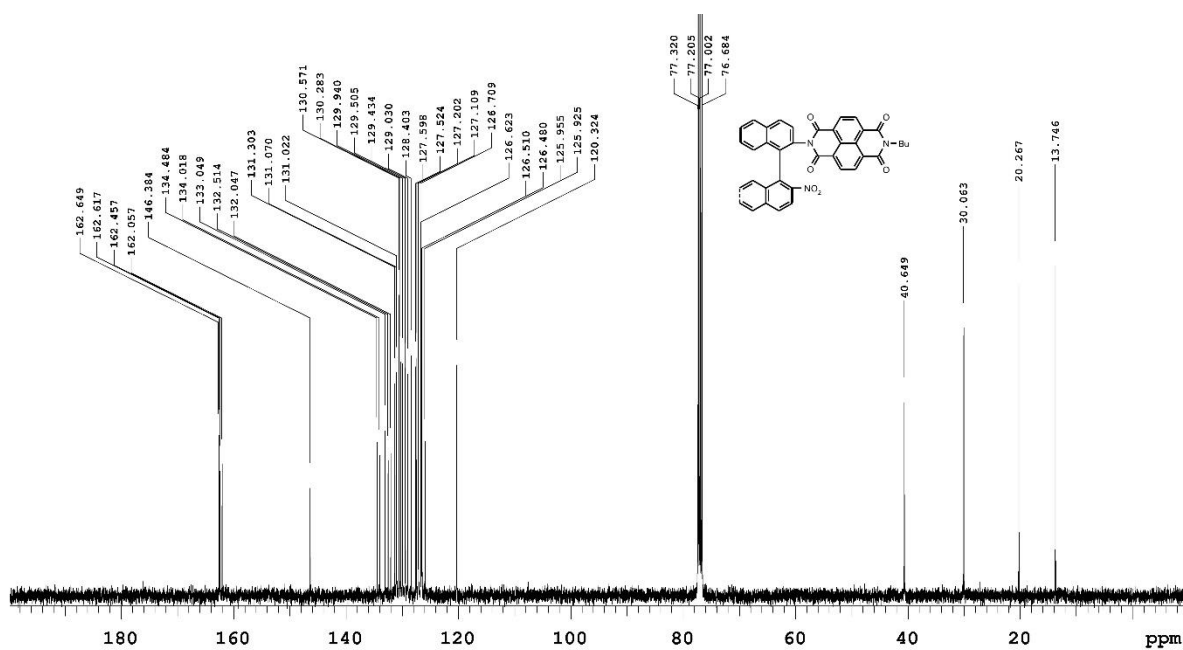
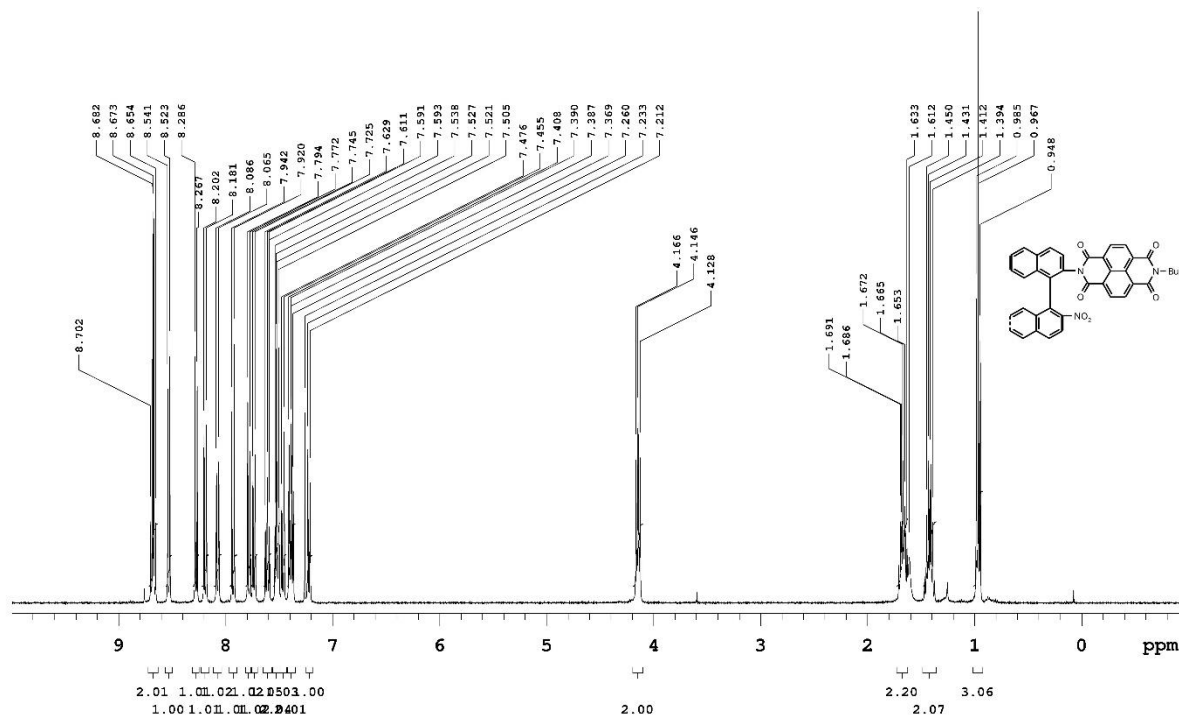


To a solution of **(S)-NDIB-NH<sub>2</sub>** (85 mg, 0.144 mmol) in CH<sub>2</sub>Cl<sub>2</sub> (5 mL) was added MCPBA (202 mg, 0.823 mmol). The mixture was stirred at rt for 16 h. The solution was washed with a saturated NaHCO<sub>3</sub>. The organic layer was dried over MgSO<sub>4</sub>, filtered and evaporated. The residue was purified by silica gel chromatography in CH<sub>2</sub>Cl<sub>2</sub>-methanol (200:1, v/v) to give 45 mg (50 %) of beige solid.

<sup>1</sup>H NMR (400MHz, CDCl<sub>3</sub>) d = 8.69 (1/2AB, J = 7.7 Hz, 1 H), 8.67 (1/2AB, J = 7.7 Hz, 1 H), 8.53 (d, J = 7.5 Hz, 1 H), 8.28 (d, J = 7.7 Hz, 1 H), 8.19 (d, J = 8.7 Hz, 1 H), 8.08 (d, J = 8.3 Hz, 1 H), 7.93 (d, J = 8.9 Hz, 1 H), 7.78 (d, J = 9.1 Hz, 1 H), 7.74 (d, J = 8.1 Hz, 1 H), 7.61 (t, J = 7.3 Hz, 1 H), 7.55 - 7.49 (m, 2 H), 7.49 - 7.44 (m, 1 H), 7.42 - 7.35 (m, 2 H), 7.22 (d, J = 8.5 Hz, 1 H), 4.18 - 4.11 (m, 2 H), 1.72 - 1.62 (m, 2 H), 1.42 (sex, J = 7.4 Hz, 2 H), 0.97 (t, J = 7.4 Hz, 3 H).

<sup>13</sup>C NMR (100MHz, CDCl<sub>3</sub>) d = 162.64, 162.61, 162.4, 162.1, 146.4, 134.5, 134.0, 133.0, 132.5, 132.0, 131.3, 131.1, 131.0, 130.57, 130.55, 130.3, 129.9, 129.5, 129.4, 129.0, 128.4, 127.6, 127.5, 127.2, 127.1, 126.70 (2x), 126.62, 126.60, 126.50, 126.48, 125.95, 125.92, 120.3, 40.7, 30.1, 20.3, 13.7.

HRMS (ESI) m/z calcd for C<sub>38</sub>H<sub>29</sub>N<sub>4</sub>O<sub>6</sub> (M+NH<sub>4</sub>)<sup>+</sup> 637.2082. Found: 637.2084.





## 2 X-ray crystallography

The suitable crystals for X-ray diffraction measurements were only obtained for NDIB-X compounds with -NHCH<sub>3</sub>, -OCH<sub>3</sub> and -NO<sub>2</sub> substituents recrystallized from toluene (NDIB-NHCH<sub>3</sub>·1.5C<sub>7</sub>H<sub>8</sub>, NDIB-OCH<sub>3</sub>·1.5C<sub>7</sub>H<sub>8</sub> and NDIB-NO<sub>2</sub>) and methanol (NDIB-OCH<sub>3</sub> and NDIB-NO<sub>2</sub>). Diffraction data were collected at 100 K on a Rigaku SuperNova (dual source) four circle diffractometer working with an Eos CCD detector and using a microfocus Nova X-ray source giving a mirror-monochromated Cu K $\alpha$  radiation ( $\lambda = 1.54184 \text{ \AA}$ ). For all operations (data collection, cell refinement, data reduction and multi-scan absorption correction) CrysAlis PRO software was used. The structures were solved by direct methods and refined by a full-matrix least-squares technique on F<sup>2</sup> data using SHELXTL programs<sup>3</sup> adapted to the OLEX2 crystallographic software.<sup>4</sup> Most non-hydrogen atoms were refined anisotropically. Hydrogen atoms bonded to carbon atoms were inserted in calculated positions and refined isotropically as a riding model in accordance with accepted rules. The hydrogen atom bound to nitrogen atom in NDIB-NHCH<sub>3</sub> was located from a difference Fourier map and its position was freely refined. Due to a disorder, two solvent molecules in both crystal structures of toluene solvates were placed in voids with an electron density corresponding to the toluene molecules. These solvent molecules were restrained with common SHELX commands using the fragmentDB tool in the OLEX2 program and finally refined isotropically. In the case of pure NDIB-OCH<sub>3</sub> and NDIB-NO<sub>2</sub> compounds the n-butyl groups are disordered over two positions with dominant occupancies refined to 0.578(16) (OCH<sub>3</sub>) and 0.709(10) or 0.507(14) (NO<sub>2</sub>). In addition, for the pure OCH<sub>3</sub> analogue, the methyl part of the methoxy group is disordered over two sites with dominant occupancies of 0.52(5). Selected details concerning the data collections and refinements are given in Table S1. The structural data for four crystals: NDIB-NHCH<sub>3</sub>·1.5C<sub>7</sub>H<sub>8</sub>, NDIB-OCH<sub>3</sub>·1.5C<sub>7</sub>H<sub>8</sub>, NDIB-OCH<sub>3</sub> and NDIB-NO<sub>2</sub> were deposited at the Cambridge Crystallographic Data Centre: CCDC-2116384, CCDC-2116385, CCDC-2116386 and CCDC-2116387, respectively.

In the case of the NDIB-OCH<sub>3</sub> compound, it was possible to obtain crystals of its solvate during recrystallization in toluene (**2**, Fig. S1) and crystals of pure compound in methanol (**3**, Fig. S1). For the NHCH<sub>3</sub> derivative, only the corresponding crystals of its toluene solvate (**1**, Fig. S1) were obtained. In turn, the use of both toluene or methanol led to the crystallization of the pure NO<sub>2</sub> analogue (**4**, Fig. S1).

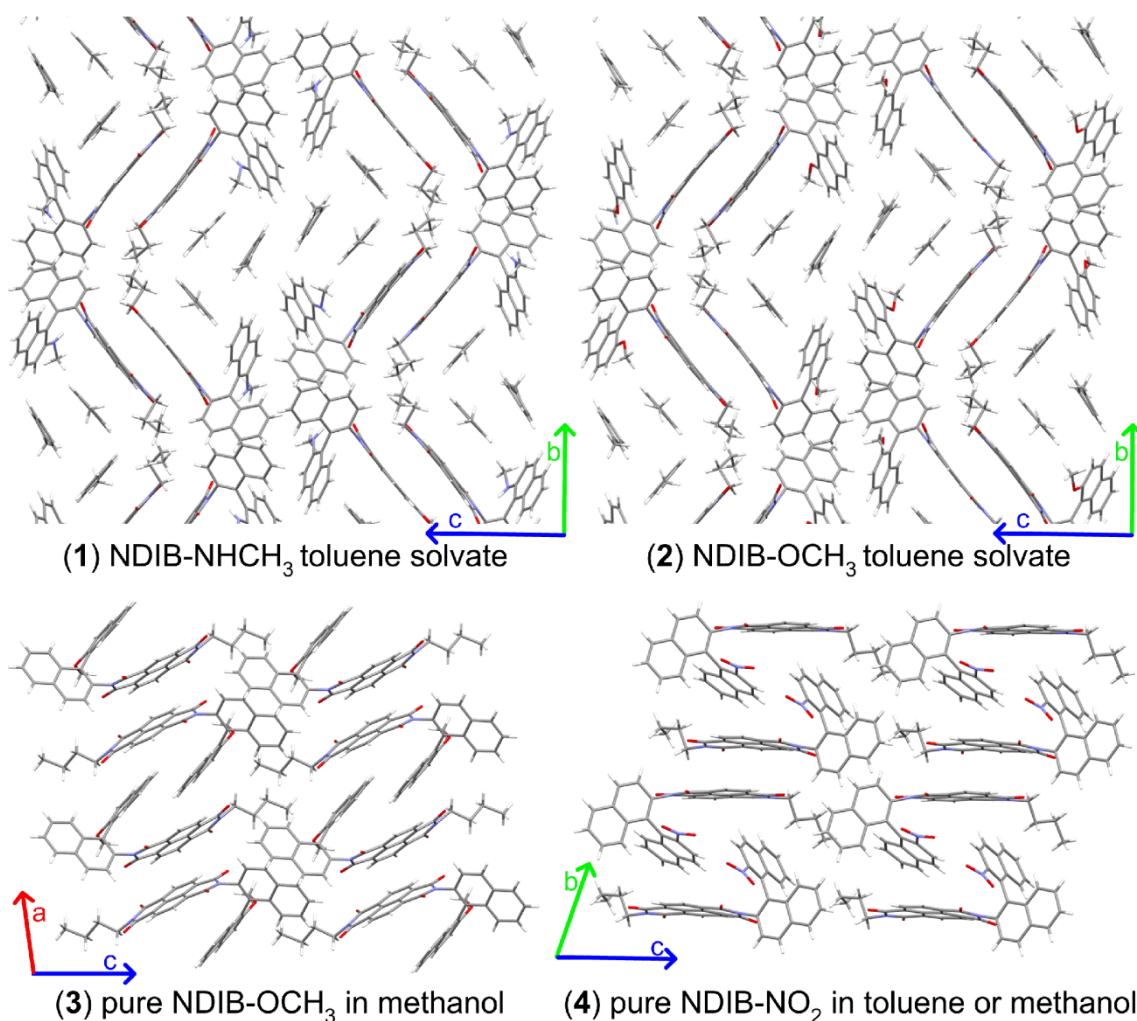
In all molecular structures of studied compounds the naphthalene part directly connected to naphthalenediimide core is almost perpendicular to it with the dihedral angle in the range of 82–88° (88° and 86° for **1**, 84° and 85° for **2**, 82° for **3** and 84° and 88° for **4**). The second naphthalene moiety forms with the naphthalenediimide fragment the lower dihedral angles of approximately 62° and 67° for **1**, 58° and 65° for **2**, 28° for **3** and 36° and 59° for **4**.

Both toluene solvates **1** and **2** display the same molecular packing crystallizing in the orthorhombic  $P2_12_12_1$  space group. Their crystal structures are composed of NDIB-X (X - NHCH<sub>3</sub> or OCH<sub>3</sub>) and solvent molecules in the 2:3 molar ratio, respectively. The naphthalenediimide fragments of NDIB-X molecules are located along the *a* axis on two adjacent approximately parallel planes, forming characteristic sheets ending with butyl groups on one side and binaphthalene moieties on the other side (Fig. S1). The neighbouring naphthalenediimide rings in **1** and **2** are stabilized by the C $\cdots$ O and  $\pi\cdots\pi$  intermolecular interactions and the shortest C $\cdots$ C and C $\cdots$ O distances between adjacent naphthalenediimide cores are presented in Fig. S2. The shortest intermolecular contact between the centroids of the aromatic rings (Cg1 $\cdots$ Cg2) is very similar in NDIB-NHCH<sub>3</sub> (3.507 Å) and NDIB-OCH<sub>3</sub> (3.498 Å) (Fig. S2). Extended crystal lattices are mainly stabilized by the formation of intermolecular C–H $\cdots$ O hydrogen bonds (Figs S3 and S4). Significant empty spaces between the NDIB-NHCH<sub>3</sub> and NDIB-OCH<sub>3</sub> molecules are occupied through toluene molecules, which stabilize the crystal structure (Fig. S1). Two toluene rings are parallel to the naphthalenediimide rings with the shortest distances between the suitable centroids equal to 3.63 (Cg1 $\cdots$ Cg1t) and 3.66 Å (Cg1 $\cdots$ Cg2t) for the NHCH<sub>3</sub> analogue, and 3.64 (Cg1 $\cdots$ Cg1t) and 3.68 Å (Cg1 $\cdots$ Cg2t) for the OCH<sub>3</sub> derivative (Fig. S2).

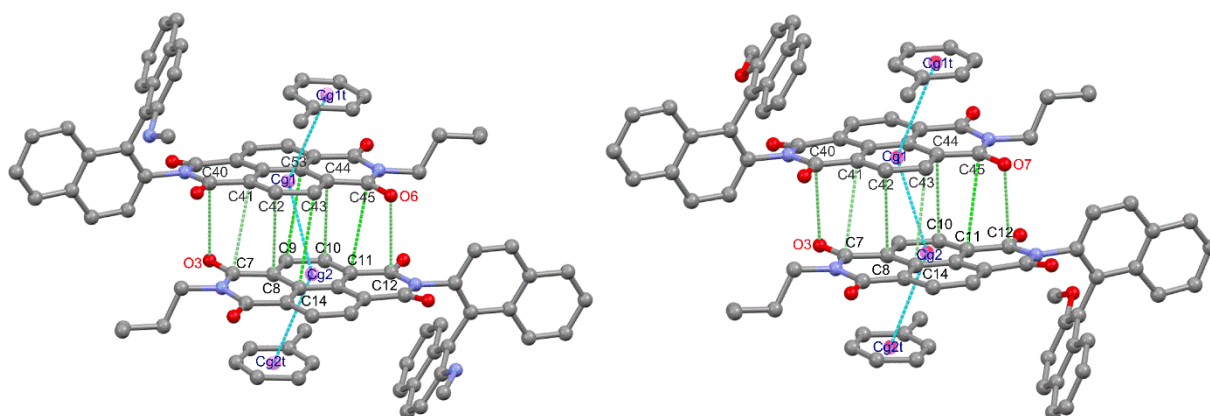
The crystal structures of **3** and **4** contain molecules of OCH<sub>3</sub> and NO<sub>2</sub> analogues crystallized without solvent molecules (Fig. S1) in the monoclinic  $P2_1$  and triclinic  $P1$  space groups, respectively. In **3** the molecules are stabilized in chains along the *b* axis through C–H $\cdots$ O intermolecular hydrogen bonds (C4–H4 $\cdots$ O3 = 3.200(5) Å and C10–H10 $\cdots$ O1 = 3.234(5) Å) (Fig. S5). Moreover, other similar contacts are also observed between adjacent chains (C20–H20 $\cdots$ O4 = 3.163(5) Å, C21–H21 $\cdots$ O4 = 3.248(4) Å, C19–H19 $\cdots$ O2 = 3.371(5) Å and C39A–H39B $\cdots$ O5 = 3.382(5) Å) (Fig. S5). The crystal structure of **3** is the only one of the presented structures which does not contain  $\pi\cdots\pi$  stabilizing interactions. The shortest distances between the centroids of the naphthalenediimide rings are equal to about 4.14 and 4.55 Å. In turn, similarly to the crystal structures of both solvates, the molecules in **4** are held in pairs by  $\pi\cdots\pi$  interactions between neighbouring naphthalenediimide parts. The contacts between centroids of the adjacent rings are equal to 3.37, 3.48 and 3.56 Å (Fig. S6). In addition, the carbonyl and nitro groups are involved in the crystal structure stabilization through the formation of the intermolecular C–H $\cdots$ O hydrogen bonds and C $\cdots$ O contacts (Fig. S7).

**Table S1.** Crystal data and structure refinement details for NDIB-X compounds.

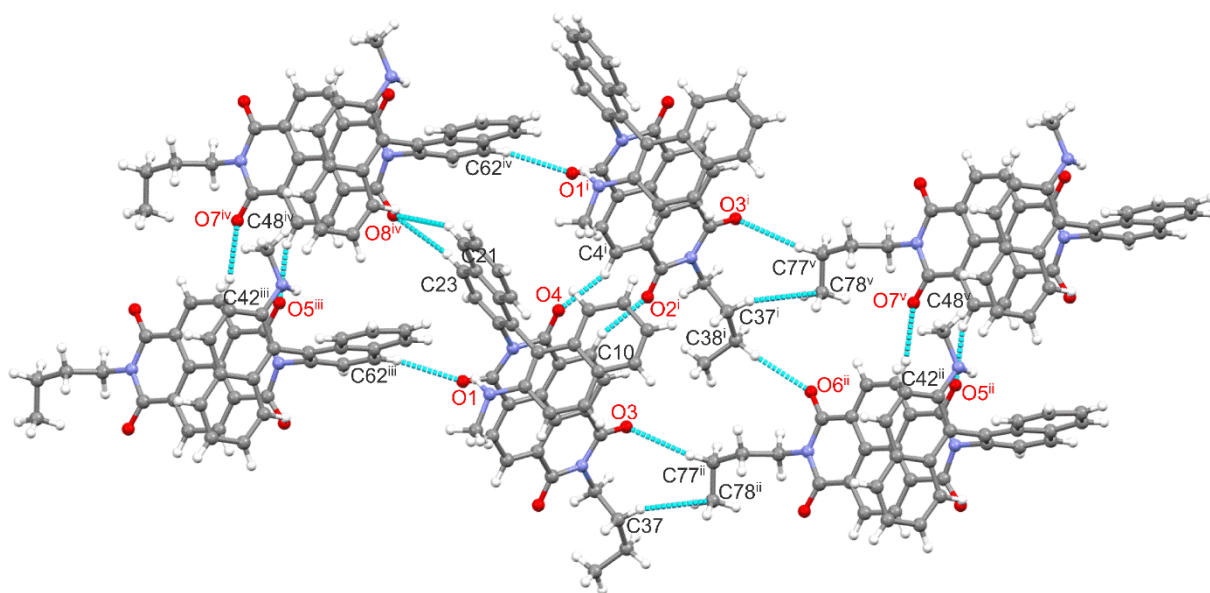
	NDIB-NHCH <sub>3</sub> ·1.5C <sub>7</sub> H <sub>8</sub> (1)	NDIB-OCH <sub>3</sub> ·1.5C <sub>7</sub> H <sub>8</sub> (2)	NDIB-OCH <sub>3</sub> (3)	NDIB-NO <sub>2</sub> (4)
Empirical formula	C <sub>99</sub> H <sub>82</sub> N <sub>6</sub> O <sub>8</sub>	C <sub>99</sub> H <sub>80</sub> N <sub>4</sub> O <sub>10</sub>	C <sub>39</sub> H <sub>28</sub> N <sub>2</sub> O <sub>5</sub>	C <sub>38</sub> H <sub>25</sub> N <sub>3</sub> O <sub>6</sub>
Moiety formula	2(C <sub>39</sub> H <sub>29</sub> N <sub>3</sub> O <sub>4</sub> )·3(C <sub>7</sub> H <sub>8</sub> )	2(C <sub>39</sub> H <sub>28</sub> N <sub>2</sub> O <sub>5</sub> )·3(C <sub>7</sub> H <sub>8</sub> )	C <sub>39</sub> H <sub>28</sub> N <sub>2</sub> O <sub>5</sub>	C <sub>38</sub> H <sub>25</sub> N <sub>3</sub> O <sub>6</sub>
Formula weight	1483.70	1485.67	604.63	619.61
Recrystallization solvent	toluene	toluene	methanol	toluene, methanol
T (K)	100.0(1)	100.0(1)	100.0(1)	100.0(1)
λ (Cu Kα) (Å)	1.54184	1.54184	1.54184	1.54184
Crystal system	orthorhombic	orthorhombic	monoclinic	triclinic
Space group	<i>P</i> 2 <sub>1</sub> 2 <sub>1</sub> 2 <sub>1</sub>	<i>P</i> 2 <sub>1</sub> 2 <sub>1</sub> 2 <sub>1</sub>	<i>P</i> 2 <sub>1</sub>	<i>P</i> 1
<i>a</i> (Å)	9.04517(12)	9.03641(8)	11.8341(3)	8.83471(17)
<i>b</i> (Å)	24.0736(3)	24.18309(19)	8.3172(2)	11.9486(3)
<i>c</i> (Å)	36.4747(5)	36.1172(4)	14.9538(5)	15.9837(4)
α (deg)	90	90	90	69.204(2)
β (deg)	90	90	98.765(3)	78.6911(18)
γ (deg)	90	90	90	75.309(2)
V (Å <sup>3</sup> )	7942.37(17)	7892.63(12)	1454.67(7)	1515.25(7)
Z	4	4	2	2
D <sub>calc.</sub> (g·cm <sup>-3</sup> )	1.241	1.250	1.380	1.358
μ (mm <sup>-1</sup> )	0.626	0.643	0.741	0.762
F(000)	3128	3128	632	644
Crystal size (mm)	0.25 x 0.08 x 0.04	0.24 x 0.12 x 0.04	0.32 x 0.10 x 0.05	0.25 x 0.18 x 0.10
Measured reflections	27455	34067	11660	64114
Unique reflections	13818	13763	4920	9583
reflections <i>I</i> > 2σ( <i>I</i> )	12824	12788	4450	9360
<i>R</i> <sub>(int)</sub>	0.0197	0.0219	0.0263	0.0373
Data/restraints/parameters	13818/ 112/ 963	13763/ 112/ 955	4920/ 1/ 449	9583/ 3/ 890
Goodness-of-fit	1.046	1.040	1.023	1.024
Final <i>R</i> <sub>1</sub> , <i>wR</i> <sub>2</sub> [ <i>I</i> > 2σ( <i>I</i> )]	0.0592, 0.1684	0.0608, 0.1746	0.0462, 0.1214	0.0354, 0.0945
Final <i>R</i> <sub>1</sub> , <i>wR</i> <sub>2</sub> (all data)	0.0637, 0.1738	0.0653, 0.1799	0.0526, 0.1273	0.0362, 0.0957
Max. peak/hole (e <sup>-</sup> ·Å <sup>-3</sup> )	1.023/-0.595	0.872/-0.547	0.553/-0.257	0.456/-0.287



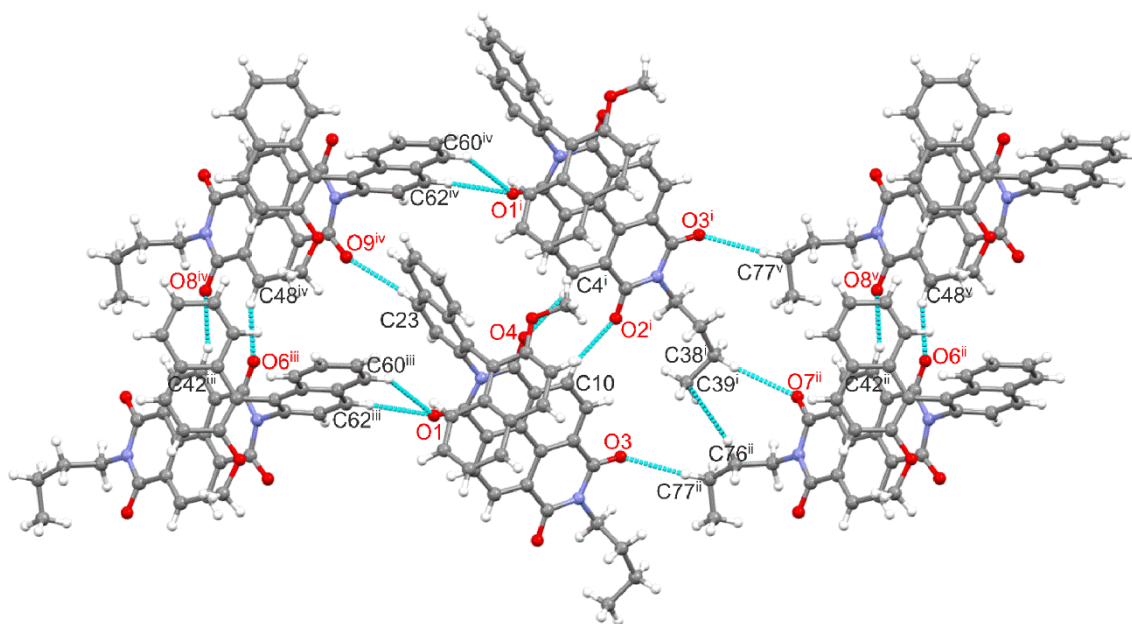
**Figure S1.** Fragments of the crystal structures of the (*R*)-NHCH<sub>3</sub>, (*S*)-OCH<sub>3</sub> and (*S*)-NO<sub>2</sub> analogues of binaphthalenyamine of *N*-butyl naphthalenediimide.



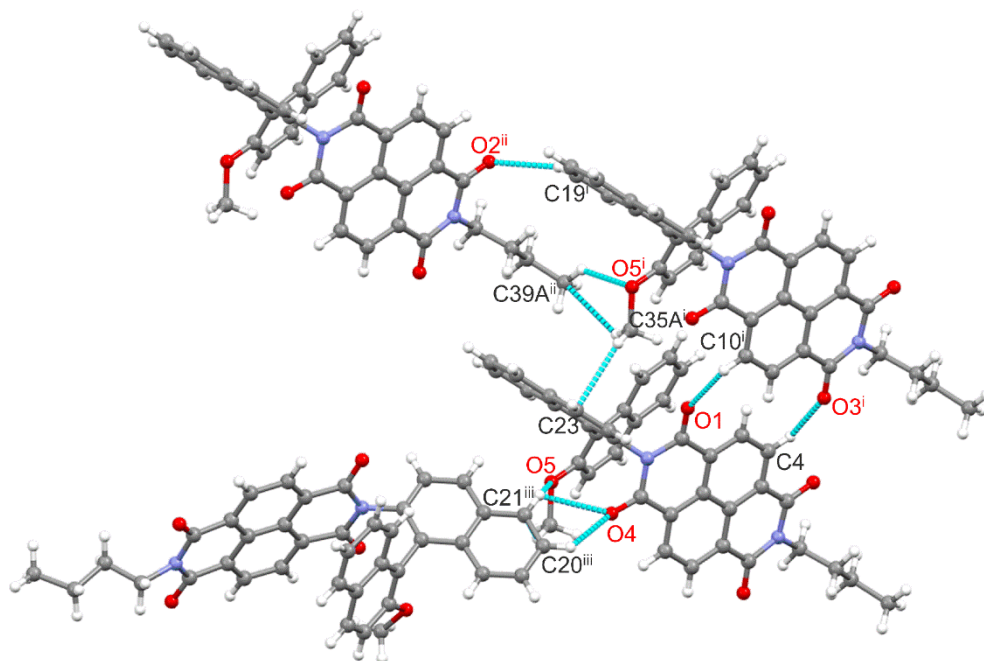
**Figure S2.** Crystal structure fragments of **1** (*R*)-NHCH<sub>3</sub>-toluene solvates, left) and **2** (*S*)-OCH<sub>3</sub>-toluene solvates, right) showing the C...O and  $\pi$ ... $\pi$  intermolecular interactions and the shortest distances between centroids of neighbouring aromatic rings (**left**: C7...C41 = 3.372(5) Å, C8...C42 = 3.439(5) Å, C9...C53 = 3.357(5) Å, C10...C44 = 3.352(5) Å, C11...C45 = 3.308(5) Å, C14...C43 = 3.481(5) Å, C12...O6 = 3.169(5) Å and C40...O3 = 3.204(5) Å; **right**: C7...C41 = 3.306(5) Å, C8...C42 = 3.368(6) Å, C10...C44 = 3.420(6) Å, C11...C45 = 3.347(6) Å, C14...C43 = 3.370(6) Å, C12...O7 = 3.203(5) Å and C40...O3 = 3.161(5) Å). Hydrogen atoms are omitted for clarity.



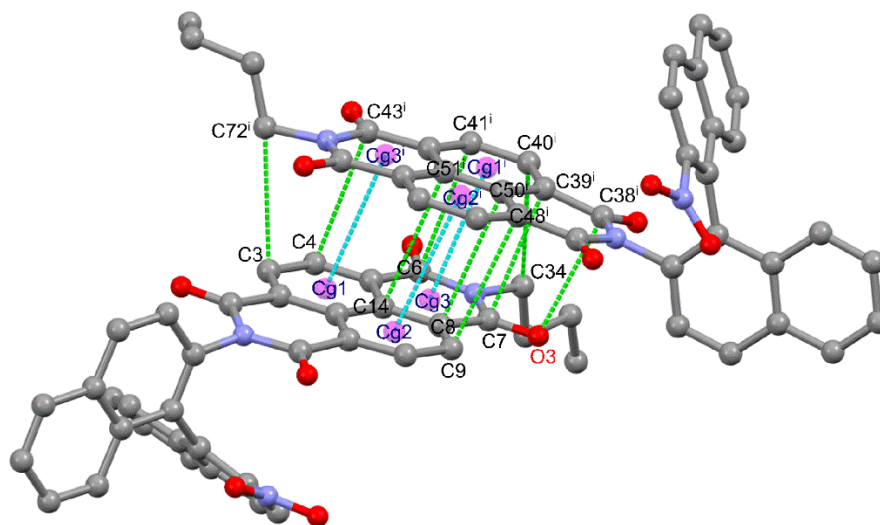
**Figure S3.** Crystal structure fragment of **1** ((*R*)-NHCH<sub>3</sub>-toluene solvates) showing the chosen intermolecular contacts between the molecules of NDIB-NHCH<sub>3</sub> (C62–H62···O1 = 3.503(5) Å, C38–H38B···O6 = 3.449(5) Å, C4–H4···O4 and C10–H10···O2 = 3.102(5) Å, C48–H48···O5 = 3.128(5) Å, C42–H42···O7 = 3.130(5) Å, C23–H23···O8 = 3.411(4) Å, C21–H21···O8 = 3.488(5) Å, C77–H77A···O3 = 3.542(2) Å and C37–H37B···C78 = 3.672(6) Å; symmetry codes: *i* = *x*+1, *y*, *z*; *ii* = *-x*+2, *y*+0.5, *-z*+1.5; *iii* = *-x*+1, *y*-0.5, *-z*+1.5; *iv* = *-x*+2, *y*-0.5, *-z*+1.5; *v* = *-x*+3, *y*+0.5, *-z*+1.5). Toluene molecules are omitted for clarity.



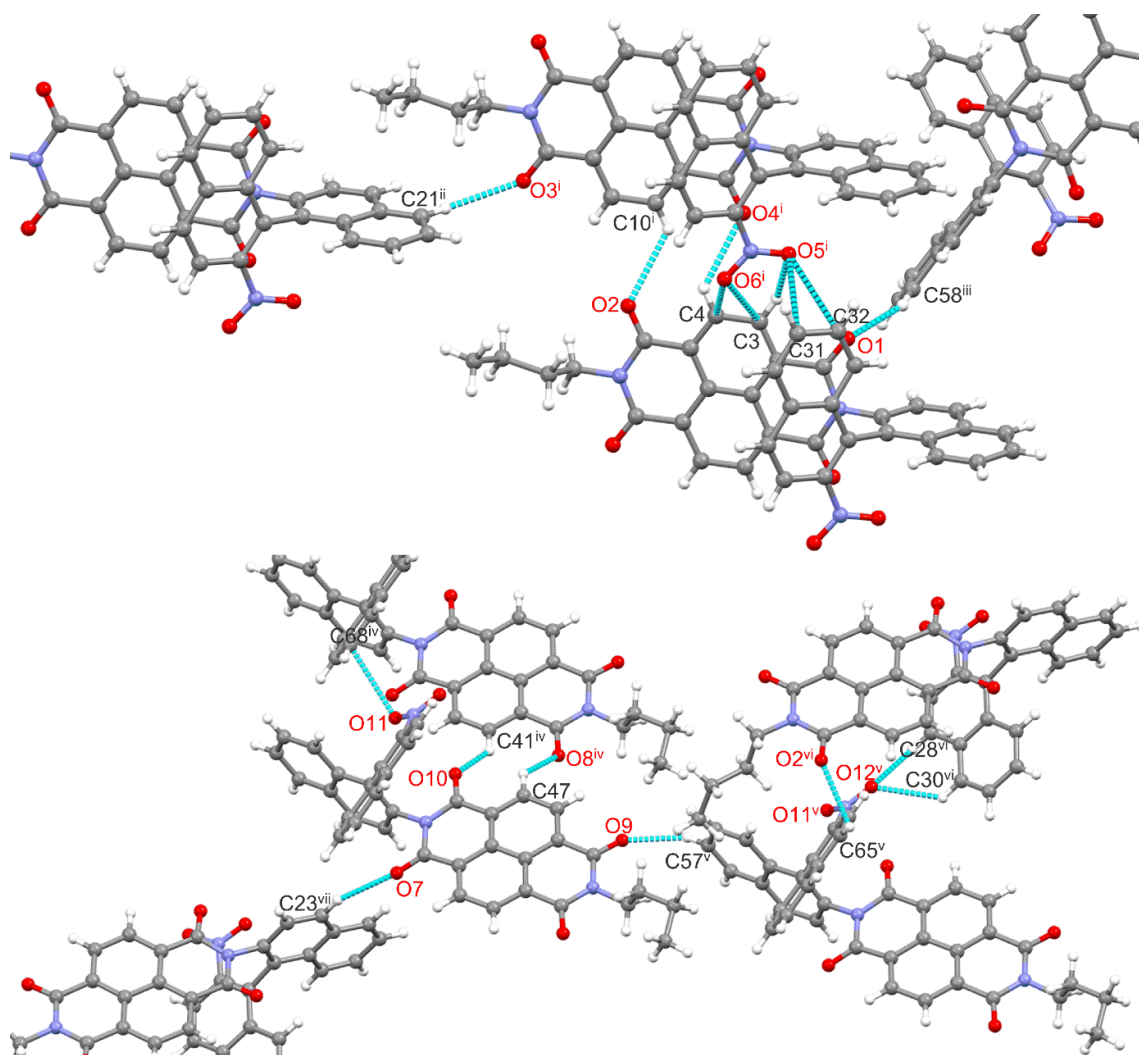
**Figure S4.** Crystal structure fragment of **2** ((*S*)-OCH<sub>3</sub>-toluene solvates) showing the chosen intermolecular contacts between the molecules of NDIB-OCH<sub>3</sub> (C48–H48···O6 = 3.094(5) Å, C42–H42···O8 = 3.102(5) Å, C10–H10···O2 = 3.109(5) Å, C4–H4···O4 = 3.113(5) Å, C23–H23···O9 = 3.383(5) Å, C62–H62···O1 = 3.402(5) Å, C77–H77A···O3 = 3.484(5) Å, C38–H38B···O7 = 3.539(5) Å; symmetry codes: *i* = *x*-1, *y*, *z*; *ii* = *-x*, *y*+0.5, *-z*+0.5; *iii* = *-x*+1, *y*-0.5, *-z*+0.5; *iv* = *-x*, *y*-0.5, *-z*+0.5; *v* = *-x*-1, *y*+0.5, *-z*+0.5). Toluene molecules are omitted for clarity.



**Figure S5.** Crystal structure fragment of **3** ((*S*)-OCH<sub>3</sub> in methanol) showing the chosen intermolecular contacts between the neighbouring NDIB-OCH<sub>3</sub> molecules (symmetry codes: *i* = *x*, *y*+1, *z*; *ii* = *x*, *y*+1, *z*-1; *iii* = -*x*+1, *y*-0.5, -*z*).



**Figure S6.** Crystal structure fragment of **4** ((*S*)-NO<sub>2</sub> in methanol or toluene) showing the shortest distances between atoms and centroids of neighbouring rings (C4...C43<sup>i</sup> = 3.370(5) Å, C6...C41<sup>i</sup> = 3.265(4) Å, C7...C39<sup>i</sup> = 3.311(4) Å, C8...C50<sup>i</sup> = 3.440(4) Å, C9...C48<sup>i</sup> = 3.473(4) Å, C14...C51<sup>i</sup> = 3.503(4) Å, C34...C40<sup>i</sup> = 3.311(4) Å, C3...C72<sup>i</sup> = 3.359(5) Å and O3...C38<sup>i</sup> = 3.1481(3) Å, Cg1...Cg3<sup>i</sup> = 3.48 Å, Cg2...Cg2<sup>i</sup> = 3.56 Å and Cg3...Cg1<sup>i</sup> = 3.37 Å; symmetry code: *i* = *x*, *y*+1, *z*). Hydrogen atoms are omitted for clarity.



**Figure S7.** Crystal structure fragments of **4** ((*S*)-NO<sub>2</sub> in methanol or toluene) showing the chosen intermolecular contacts between the neighbouring NDIB-NO<sub>2</sub> molecules (**top**: C58–H58···O1 = 3.221(4) Å, C10–H10···O2 = 3.366(3) Å, C21–H21···O3 = 3.421(3) Å, C4–H4···O4 = 3.359(3) Å, C3–H3···O5 = 3.466(3) Å, O6···C4 = 3.014(4) Å, O6···C4 = 3.108(4) Å, O5···C31 = 3.133(4) Å and O5···C32 = 3.152(4) Å; **bottom**: C23–H23···O7 = 3.590(3) Å, C47–H47···O8 = 3.139(4) Å, C57–H57···O9 = 3.182(4) Å, C41–H41···O10 = 3.034(4) Å, C30–H30···O12 = 3.292(5) Å, C28–H28···O12 = 3.324(5) Å, C65–H65···O2 = 3.124(4) Å and O11···C68 = 3.134(4) Å; symmetry codes: *i* = *x*+1, *y*, *z*; *ii* = *x*+1, *y*, *z*+1; *iii* = *x*+1, *y*+1, *z*-1; *iv* = *x*-1, *y*, *z*; *v* = *x*+1, *y*, *z*-1; *vi* = *x*, *y*, *z*-1; *vii* = *x*, *y*-1, *z*+1).

### 3. DFT calculations of the substituent effect

**Geometry optimization:** Structures of the NDIB-X molecule were optimized using the CAM-B3LYP functional<sup>5</sup> with the Grimme's D3 dispersion correction<sup>6</sup> and different basis sets depend on the simulation aim: TZVP<sup>7,8</sup> for the study of substituent effect, def2-TZVP<sup>9,10</sup> for the study of conformer of the five derivatives studied experimentally. The Gaussian 09 package<sup>11</sup> was applied for the quantum-chemical calculations and GaussView<sup>12</sup> for the visualization. The stationary structures were found by ascertaining that all harmonic frequencies were real.

**Calculation of the substituent effect sEDA and pEDA descriptors:** The sEDA and pEDA descriptors for the NDIB-X molecules reveal the influence of the substituent on the  $\sigma$ - and  $\pi$ -valence electron systems in the ring, namely, the substituted naphthalene Ring(1), Ring(2), and the two rings together, where 1 stands for the substituted 6-membered ring. They were calculated according to Eq. 1, as in Ref. 11:<sup>13,14</sup>

$$\begin{aligned} sEDA &= \sum_{i=1}^n (\sigma_i - \sigma_{ref}) \\ pEDA &= \sum_{i=1}^n (\pi_i - \pi_{ref}) \end{aligned} \quad (1)$$

where  $\sigma_i$  and  $\pi_i$  denote  $\sigma$  or  $\pi$  valence electron populations at the  $i$ -th carbon atom in the given  $n$ -carbon atom ring (or the  $\pi$ -electron system), and the superscript *ref* denotes the respective values in the reference unsubstituted system.

Notice that positive values denote electron donating while negative electron withdrawing effect. They are given in electrons shifted to or withdrawn from the studied  $\pi$ -electron system.

The  $\sigma$ - and  $\pi$ -valence electron populations,  $p(\cdot)$ , and the sEDA and pEDA descriptors for the Ring(1), Ring(2), and the two rings together of the substituted naphthalene system in the NDIB-X molecules are gathered in Table S2. Correlations of the pEDA descriptor and the HOMO level and LUMO-HOMO gap energy, as well as position of the maximum of the first ECD band are presented in Fig. S8. Notice that the LUMO level is resistant to the substituent attached at the naphthalene system.

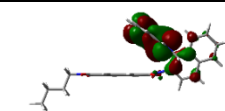
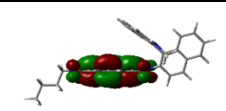
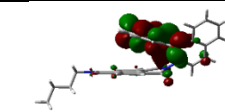
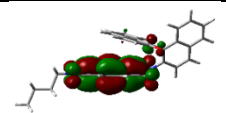
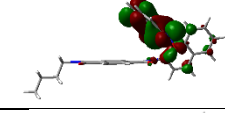
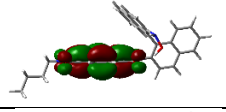
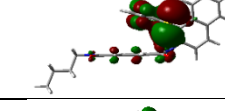
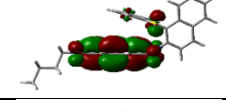
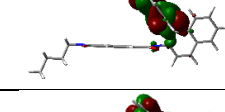
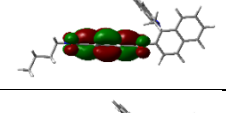
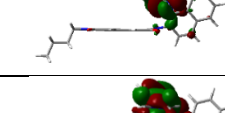
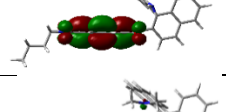
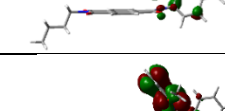
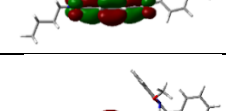
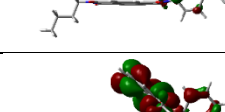
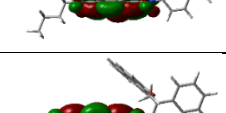




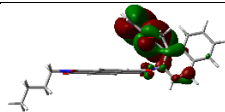
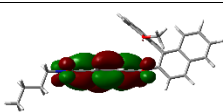
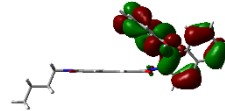
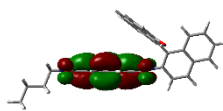
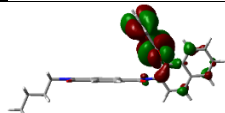
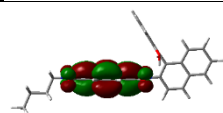
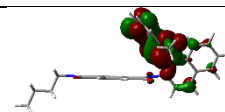
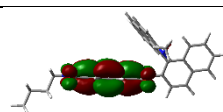
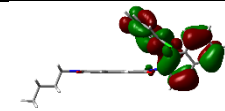
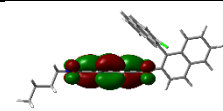

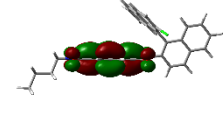
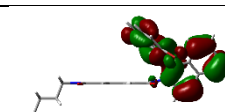
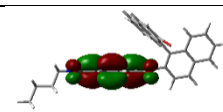
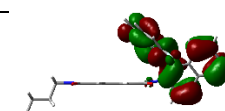
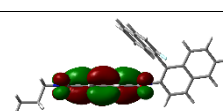
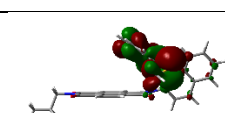
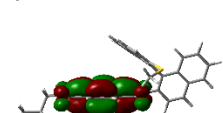
**Table S2.** DFT predicted the substituent influence of the substituent X in the NDIB-X molecules on  $\sigma$ - and  $\pi$ -electron populations in the six C-atoms of the substituted naphthalene rings, where Ring(1) and Ring(2) denote the substituted and unsubstituted ring, respectively.  $p(sp^2)$  and  $p(p_z)$  denote electron populations (in  $e$ ) of the  $\sigma$ - and  $\pi$ -orbitals, respectively, and sEDA and pEDA denotes the difference in the orbital population in the substituted and unsubstituted molecule:  $sEDA=p(sp^2)_X - p(sp^2)_H$  and  $pEDA=p(p_z)_X - p(p_z)_H$ , respectively. The calculations were done at the CAM-B3LYP/TZVP level, including the D3 Grimme correction for the dispersion forces. The rows are ordered according to the strength of the electron-donating effect on the Ring(1)  $\pi$ -electron system (in blue).

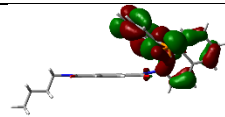
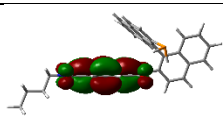
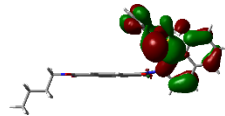
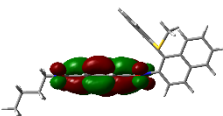
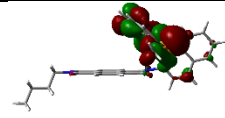
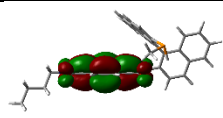
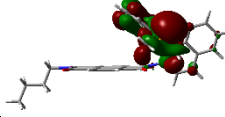
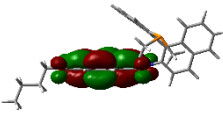
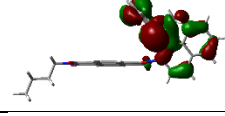
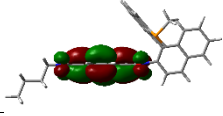
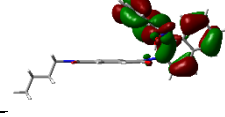
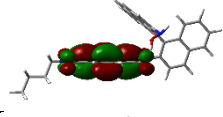
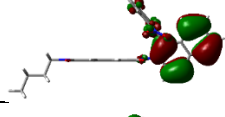
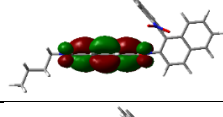
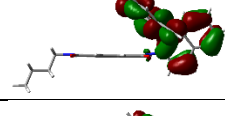
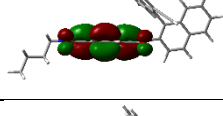
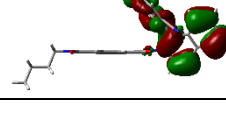
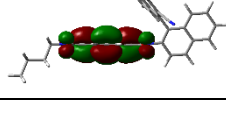
X	Ring(1)				Ring(2)				Rings (1+2)			
	$p(sp^2)$	$p(p_z)$	sEDA	pEDA	$p(sp^2)$	$p(p_z)$	sEDA	pEDA	$p(sp^2)$	$p(p_z)$	sEDA	pEDA
NHMe-2	18.211	6.134	-0.429	0.137	18.801	6.039	-0.033	0.069	37.013	12.173	-0.462	0.206
O <sup>-</sup>	18.178	6.133	-0.462	0.137	18.772	6.179	-0.063	0.209	36.950	12.312	-0.525	0.346
NHOH-1	18.251	6.117	-0.389	0.120	18.809	6.019	-0.026	0.049	37.060	12.136	-0.415	0.169
S <sup>-</sup>	18.591	6.115	-0.049	0.119	18.789	6.101	-0.045	0.131	37.381	12.217	-0.094	0.250
NHMe-1	18.234	6.115	-0.407	0.118	18.807	6.028	-0.028	0.058	37.040	12.143	-0.435	0.176
NH <sub>2</sub>	18.240	6.101	-0.400	0.105	18.808	6.023	-0.027	0.053	37.048	12.124	-0.427	0.157
NMe <sub>2</sub>	18.234	6.086	-0.407	0.089	18.798	5.995	-0.036	0.025	37.032	12.081	-0.443	0.114
nhome-2	18.272	6.080	-0.368	0.084	18.812	6.012	-0.022	0.042	37.085	12.093	-0.390	0.126
OMe-1	18.145	6.078	-0.496	0.082	18.816	6.005	-0.018	0.035	36.961	12.083	-0.514	0.117
OMe-2	18.145	6.078	-0.496	0.082	18.816	6.005	-0.018	0.035	36.961	12.083	-0.514	0.117
OH-1	18.144	6.077	-0.496	0.080	18.816	6.002	-0.018	0.032	36.961	12.079	-0.514	0.112
OH-2	18.161	6.068	-0.479	0.072	18.811	6.007	-0.023	0.037	36.972	12.075	-0.502	0.108
nhome-1	18.261	6.067	-0.380	0.071	18.813	6.006	-0.021	0.036	37.074	12.073	-0.401	0.107
Cl	18.394	6.066	-0.246	0.069	18.826	5.973	-0.008	0.003	37.220	12.039	-0.254	0.072
SH-1	18.526	6.061	-0.114	0.065	18.827	5.980	-0.008	0.010	37.353	12.042	-0.122	0.075
Br	18.461	6.061	-0.179	0.064	18.827	5.970	-0.007	0.000	37.288	12.031	-0.186	0.065
F	18.069	6.058	-0.572	0.062	18.819	5.987	-0.016	0.017	36.887	12.045	-0.587	0.079
SMe-1	18.537	6.049	-0.103	0.052	18.830	5.982	-0.005	0.012	37.367	12.031	-0.108	0.064
PH <sub>2</sub>	18.661	6.031	0.020	0.034	18.831	5.980	-0.003	0.010	37.492	12.011	0.017	0.044
SMe-2	18.548	6.030	-0.092	0.034	18.834	5.972	-0.001	0.002	37.382	12.002	-0.093	0.036
PHMe-1	18.675	6.028	0.035	0.031	18.832	5.983	-0.003	0.013	37.507	12.011	0.032	0.044
PMe <sub>2</sub>	18.688	6.026	0.047	0.030	18.829	5.989	-0.006	0.019	37.516	12.015	0.042	0.048
PHMe-2	18.687	6.018	0.047	0.022	18.834	5.974	-0.001	0.004	37.521	11.992	0.046	0.025
NHOH-2	18.315	6.010	-0.326	0.013	18.829	5.981	-0.005	0.011	37.144	11.991	-0.331	0.024
NO <sub>2</sub>	18.318	6.002	-0.322	0.006	18.839	5.928	0.004	-0.042	37.157	11.930	-0.317	-0.036
CCH	18.464	6.001	-0.176	0.005	18.837	5.965	0.003	-0.005	37.301	11.966	-0.174	0.000
CN	18.474	5.999	-0.166	0.002	18.846	5.940	0.012	-0.030	37.320	11.939	-0.154	-0.028
H	18.640	5.997	0.000	0.000	18.834	5.970	0.000	0.000	37.475	11.967	0.000	0.000
Me	18.428	5.995	-0.212	-0.001	18.828	5.990	-0.006	0.020	37.257	11.985	-0.218	0.018
tBu	18.424	5.994	-0.216	-0.003	18.823	5.990	-0.012	0.020	37.247	11.984	-0.228	0.017
SiH <sub>3</sub>	18.809	5.992	0.169	-0.005	18.841	5.968	0.007	-0.002	37.650	11.960	0.175	-0.006
PH	18.429	5.988	-0.211	-0.008	18.827	5.992	-0.008	0.022	37.256	11.980	-0.219	0.013
COOMe-1	18.504	5.984	-0.136	-0.013	18.839	5.947	0.004	-0.023	37.342	11.931	-0.132	-0.036
COMe-2	18.513	5.982	-0.128	-0.015	18.841	5.948	0.007	-0.022	37.354	11.930	-0.121	-0.037
COOH-1	18.512	5.981	-0.128	-0.016	18.843	5.942	0.009	-0.028	37.355	11.923	-0.120	-0.044
COOH-2	18.518	5.978	-0.122	-0.018	18.840	5.940	0.005	-0.029	37.358	11.919	-0.117	-0.048
COOMe-2	18.512	5.979	-0.129	-0.018	18.836	5.944	0.002	-0.025	37.348	11.923	-0.127	-0.043
COMe-1	18.529	5.973	-0.111	-0.023	18.833	5.950	-0.002	-0.020	37.362	11.923	-0.113	-0.043
CHO-2	18.520	5.971	-0.120	-0.025	18.846	5.939	0.011	-0.031	37.366	11.910	-0.109	-0.056
BF <sub>2</sub>	18.805	5.969	0.164	-0.028	18.847	5.947	0.013	-0.023	37.652	11.916	0.177	-0.051
CHO-1	18.537	5.957	-0.103	-0.040	18.845	5.947	0.010	-0.023	37.382	11.903	-0.093	-0.063
BH <sub>2</sub>	18.727	5.952	0.086	-0.044	18.826	5.992	-0.008	0.022	37.553	11.944	0.078	-0.022
BOH <sub>2</sub>	18.767	5.963	0.086	-0.044	18.840	5.964	-0.008	0.022	37.607	11.926	0.078	-0.022

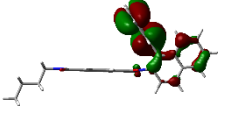
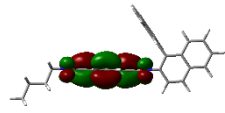
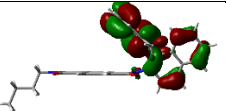
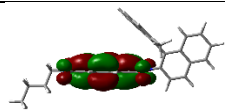

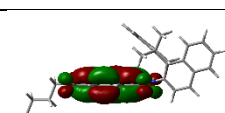
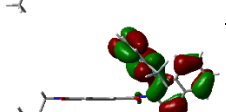
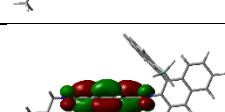
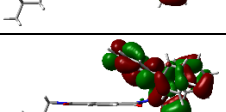
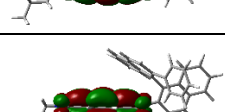
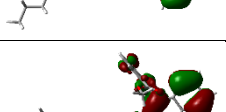
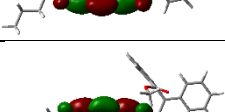
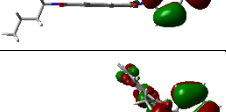
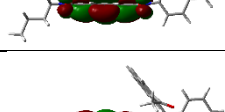

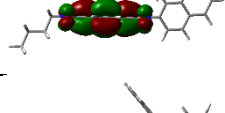
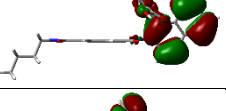
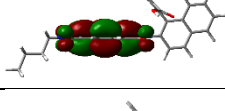



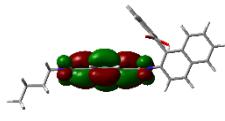
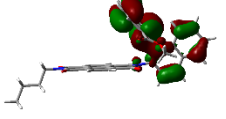
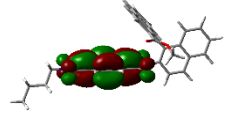
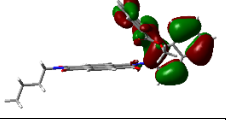
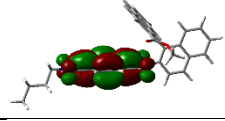
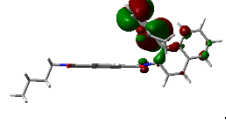
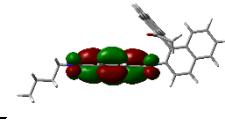
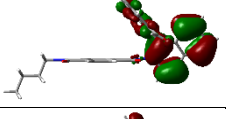
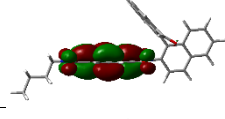
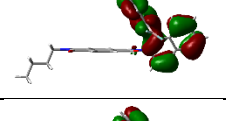
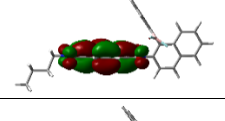
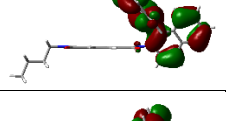
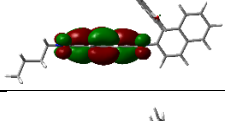
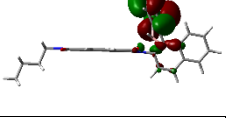
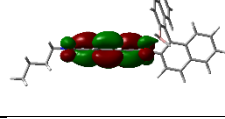
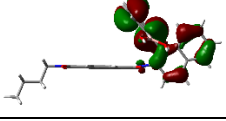
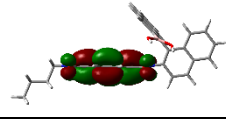
**Table S3.** The geometrical, ECD spectroscopy parameters of the lowest wavelength band, energetics of the HOMO and LUMO states, and visualization of these states calculated for substituted NDIB-X molecules at the CAM-B3LYP/TZVP level.

X	Ring 1 pEDA	$\tau_1$ (deg)	$\tau_2$ (deg)	$\lambda$ (nm)	f	R(l)	transitiion	Contribution	$E_H$	$E_L$	$E_L-E_H$	HOMO(HOMO-1,-2)	LUMO(LUMO+1)
NHMe-2	0.137	-70.75	104.17	509	0.0058	2.1	158→159	98%	-0.24202	-0.08916	0.15286		
O <sup>-</sup>	0.137	-59.66	111.90	1064	0.0409	22.8	154→155	98%	-0.10669	0.00286	0.10955		
NHOH-1	0.120	-72.93	102.70	486	0.0010	-2.0	158→159	97%	-0.25427	-0.09813	0.15614		
S	0.119	-66.79	104.60	1058	0.0859	25.5	158→159	98%	-0.10020	0.00192	0.10212		
NHMe-1	0.118	-74.30	100.76	502	0.0086	-6.0	158→159	98%	-0.24498	-0.09178	0.1532		
NH <sub>2</sub>	0.105	-74.49	101.81	466	0.0083	-5.8	154→155	98%	-0.25247	-0.09239	0.16008		
NMe <sub>2</sub>	0.089	-107.73	68.67	480	0.0291	-2.3	162→163	97%	-0.24945	-0.08955	0.1599		
nhome-2	0.084	-74.56	101.61	450	0.0078	-7.6	162→163	98%	-0.25595	-0.09287	0.16308		
OMe-1	0.082	-72.10	102.08	422	0.002	-2.1	158→159	95%	-0.26258	-0.09091	0.17167		

OMe-2b	0.082	-105.70	69.13	383	0.0204	13.7	158→159	95%	-0.26922	-0.08849	0.18073		
OH-1	0.080	-71.41	103.52	407	0.0027	-1.6	154→155	90%	-0.26556	-0.09087	0.17469		
OH-2	0.072	-76.27	99.36	421	0.0025	-5.5	154→155	98%	-0.26609	-0.09718	0.16891		
nhome-1	0.071	-75.39	104.53	432	0.0093	-7.2	162→163	98%	-0.25733	-0.09041	0.16692		
Cl	0.069	-74.86	103.99	369	0.0041	-4.2	158→159	83%	-0.27555	-0.09210	0.18345		
SH-1	0.065	-78.81	102.67	402	0.0067	-8.0	158→159	97%	-0.26786	-0.09405	0.17381		
Br	0.064	-76.15	103.28	368	0.0052	-5.1	167→168	82%	-0.27594	-0.09202	0.18392		
F	0.062	-71.62	105.99	376	0.0019	-2.9	154→155	86%	-0.27369	-0.09246	0.18123		
SMe-1	0.052	-74.53	103.41	408	0.0039	1.4	162→163	95%	-0.26529	-0.09227	0.17302		

PH <sub>2</sub>	0.034	-76.42	102.31	388	0.0048	-3.5	158→159	95%	-0.27188	-0.09224	0.17964		
SMe-2	0.034	-76.61	101.60	390	0.0029	-2.5	162→163	94%	-0.26661	-0.09071	0.1759		
PHMe-1	0.031	-76.30	102.89	402	0.0032	-1.4	162→163	96%	-0.26788	-0.09288	0.175		
PMe <sub>2</sub>	0.030	-74.06	104.35	418	0.0027	-1.5			-0.26155	-0.09319	0.16836		
PHMe-2	0.022	-80.36	97.24	388.0900	0.0046	-8.5	162→163	96%	-0.26857	-0.09129	0.17728		
NHOH-2	0.013	-79.62	97.23	389	0.0007	-1.6	158→159	85%	-0.27375	-0.09428	0.17947		
NO <sub>2</sub>	0.006	-79.00	94.01	344	0.0093	-5.9	161→162	91%	-0.28126	-0.09499	0.18627		
CCH	0.005	-75.96	103.11	377	0.0035	-2.3	156→157	89%	-0.27206	-0.09086	0.1812		
CN	0.002	-74.79	103.19	355	0.0018	-2.4	156→157	85%	-0.28041	-0.09561	0.1848		

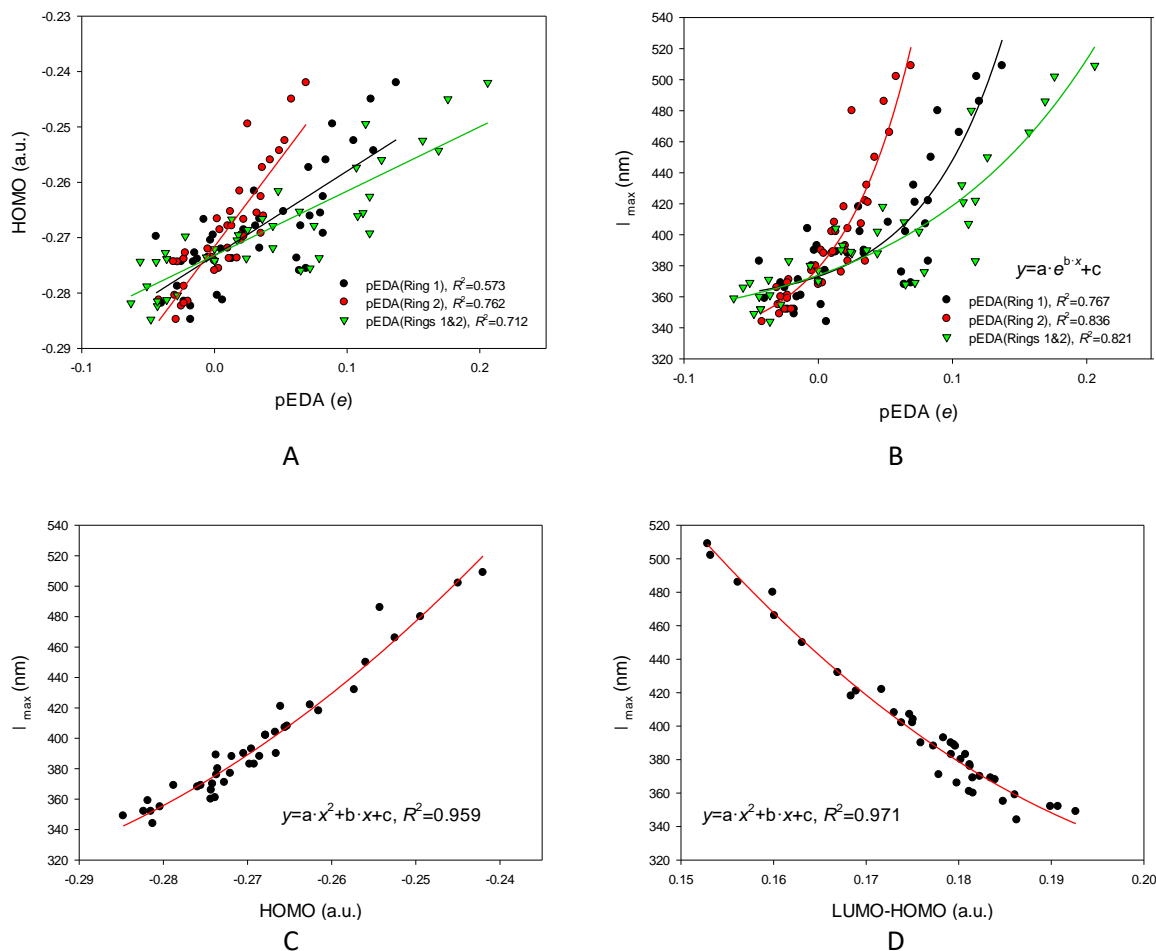
H	0.000	-84.29	87.83	370	0.0064	12.2	150→151	95%	-0.27417	-0.09189	0.18228		
Me	-0.001	-75.89	102.39	393	0.0021	-2.4	154→155	95%	-0.26954	-0.09119	0.17835		
tBu	-0.003	-81.53	99.33	390	0.0006	0.2	166→167	93%	-0.27047	-0.09131	0.17916		
SiH <sub>3</sub>	-0.005	-77.04	98.94	380	0.0016	-0.3	158→159	91%	-0.27355	-0.09332	0.18023		
PH	-0.008	-72.26	109.70	404	0.0064	2.0	170→171	91%	-0.26670	-0.09164	0.17506		
COOMe-1	-0.013	-84.52	89.59	361	0.0001	1.4	165→166	64%	-0.27385	-0.09272	0.18113		
COMe-2	-0.015	-80.43	92.64	371	0.0005	0.8	161→162	77%	-0.27276	-0.09491	0.17785		
COOH-1	-0.016	-80.60	92.49	360	0.0002	-0.4	161→162	79%	-0.27438	-0.09284	0.18154		
COOH-2	-0.018	-83.81	89.40	349	0.0080	19.6	160→162	50%	-0.28477	-0.09212	0.19265		

				338	0.1430	14.0	161→162	42%	-0.27958	-0.09212	0.18746		
COOMe-2	-0.018	-86.36	87.63	352	0.0106	27.1	164→166	61%	-0.28235	-0.09162	0.19073		
				339	0.1003	0.1	165→166	55%	-0.27929	-0.09162	0.18767		
COMe-1	-0.023	-88.62	85.02	352	0.0160	34.2	161→162	94%	-0.28149	-0.09157	0.18992		
CHO-2	-0.025	-78.54	94.30	366	0.0008	-1.4	157→158	84%	-0.27432	-0.09451	0.17981		
BF <sub>2</sub>	-0.028	-79.62	88.05	369	0.0174	1.5	161→162	65%	-0.27878	-0.09727	0.18151		
CHO-1	-0.040	-77.53	98.14	359	0.0049	-0.1	157→158	86%	-0.28185	-0.09579	0.18606		
BH <sub>2</sub>	-0.044	-81.01	73.07	466	0.0051	-2.2	153→154	96%	-0.26465	-0.10871	0.15594		
B(OH) <sub>2</sub>	-0.044			383	0.0040	11.0	161→162	89%	-0.26977	-0.09057	0.1792		

### Important correlations that demonstrate the substituent influence on $\lambda_{\max}$ first ECD band

The linear correlations between the energy of the HOMO state and the pEDA descriptor calculated for substituted naphthalene rings, Ring(1) and Ring(2), and the entire naphthalene system, Ring(1) + Ring(2), are weak but statistically significant. They show that the more charge is supplied to the naphthalene rings, positive pEDA values, the higher is the HOMO level (Figure S8A). Since, in essence, the LUMO level is substituent independent, the energy of the HOMO-LUMO transition decreases, non-linearly, with the pEDA descriptor, and thus the position of the  $\lambda_{\max}$  first ECD band increases (Figure S8B). The spread of the points around the correlation lines weakens the correlation coefficients because of an ununiform steric hindrance produced by the substituents which, sometimes, may also lead to perturbation of the NDIB-X conformation.

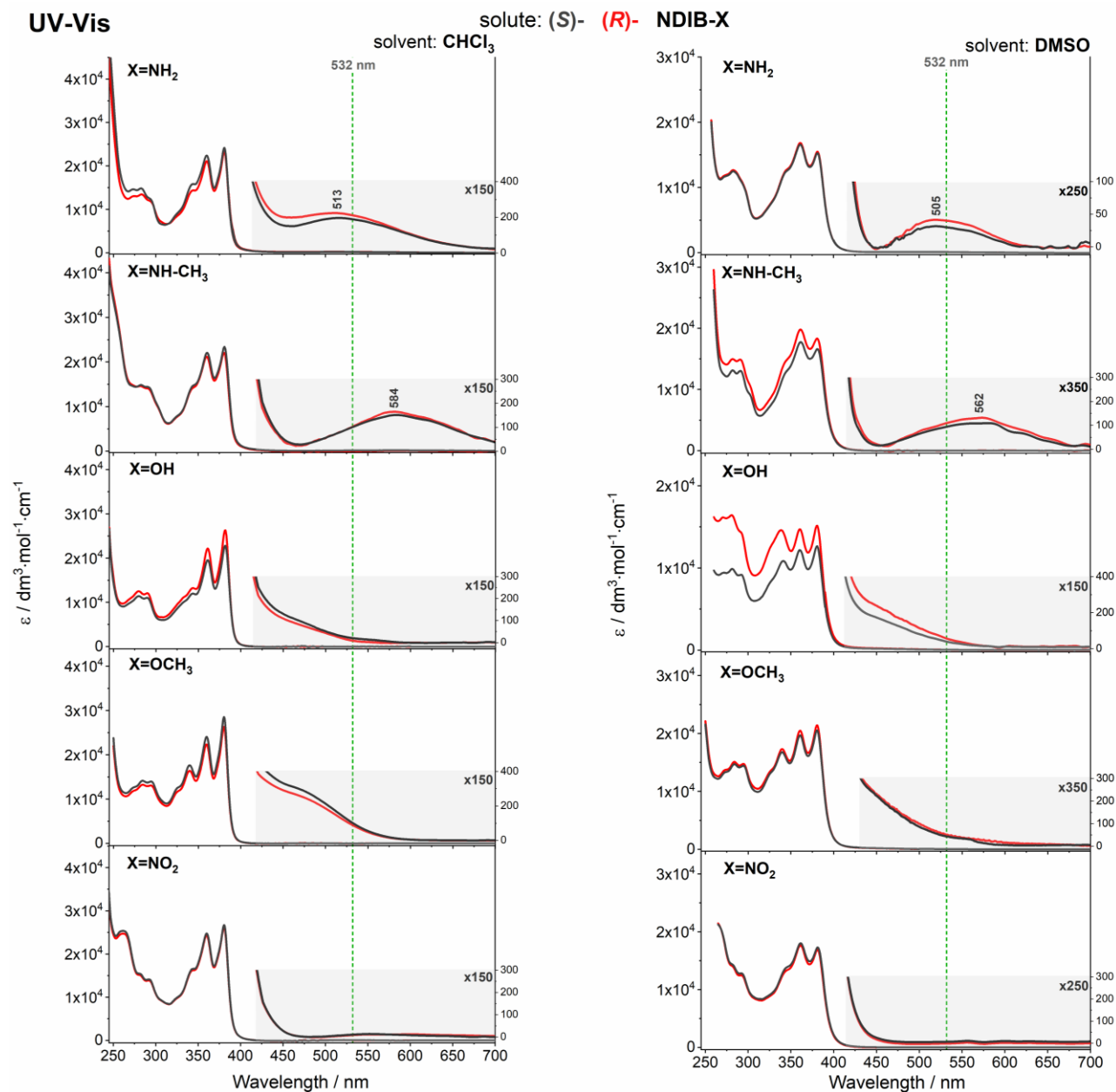
Good, slightly non-linear, correlations between the  $\lambda_{\max}$  first ECD band values and the HOMO or LUMO-HOMO energies (Figures S8C and S8D) confirm the independence of the LUMO level on the NDIB substituent.



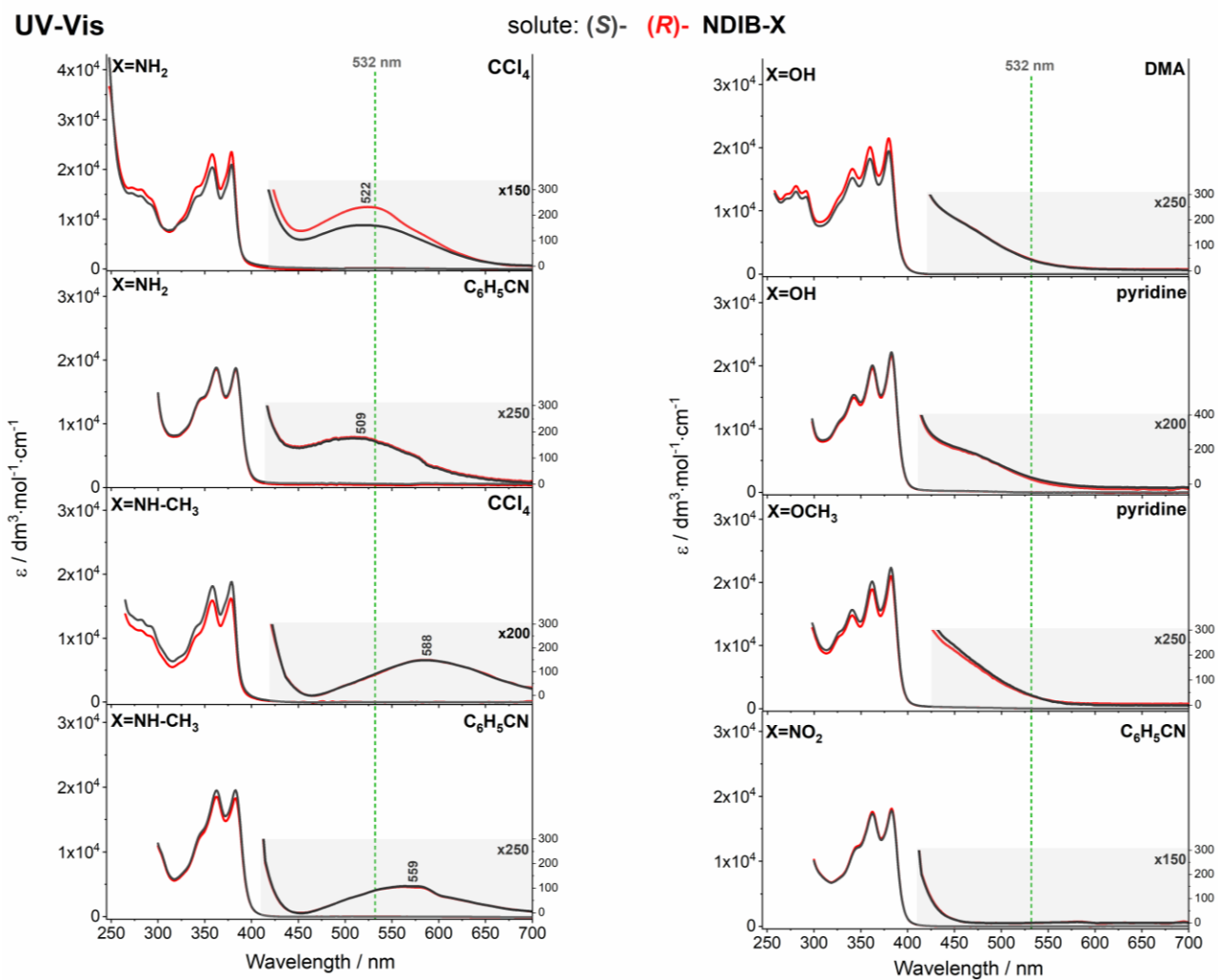
**Figure S8.** (A) Significant linear correlations between the HOMO level energy and the pEDA descriptors of the substituent positioned at the naphthalene moiety. (B) Significant non-linear (exponential) correlations between  $\lambda_{\max}$  position in the first ECD band of NDIB-X and the pEDA descriptors of the substituent positioned at the naphthalene moiety. (C) Significant quadratic correlation between  $\lambda_{\max}$  position in the first ECD band of NDIB-X and the HOMO level energy. (D) Significant quadratic correlation between  $\lambda_{\max}$  position in the first ECD band of NDIB-X and the LUMO-HOMO gap. Calculations were carried out at the CAM-B3LYP/TZVP level with the D3 Gimme's correction.

## 4 UV-Vis and ECD measurements

The ECD and UV-Vis spectra of NDIB-derivatives were recorded in the 380-700 nm spectral range at room temperature in spectroscopic grade solvents:  $\text{CHCl}_3$ ,  $\text{CCl}_4$ ,  $\text{C}_6\text{H}_5\text{CN}$ , DMSO, pyridine and *N,N*-dimethylacetamide (DMA). Solutions (ca.  $3\text{-}7 \times 10^{-4} \text{ mol/dm}^3$ ) were measured in the 1 cm quartz cell above 380 nm. The UV-Vis/ECD spectra of the NDI-derivatives were also collected below 380 nm, where the lower limit was determined by the solvents and registrations sometimes required using 0.1 cm and 0.2 cm cuvettes. All spectra were recorded on Jasco J-1500 spectropolarimeter with a  $100 \text{ nm min}^{-1}$  scanning speed, a step size of 0.2 nm, a bandwidth of 1 nm, a response time of 1 s, an accumulation of 5 scans and were background-corrected using the respective solvent recorded under the same conditions.

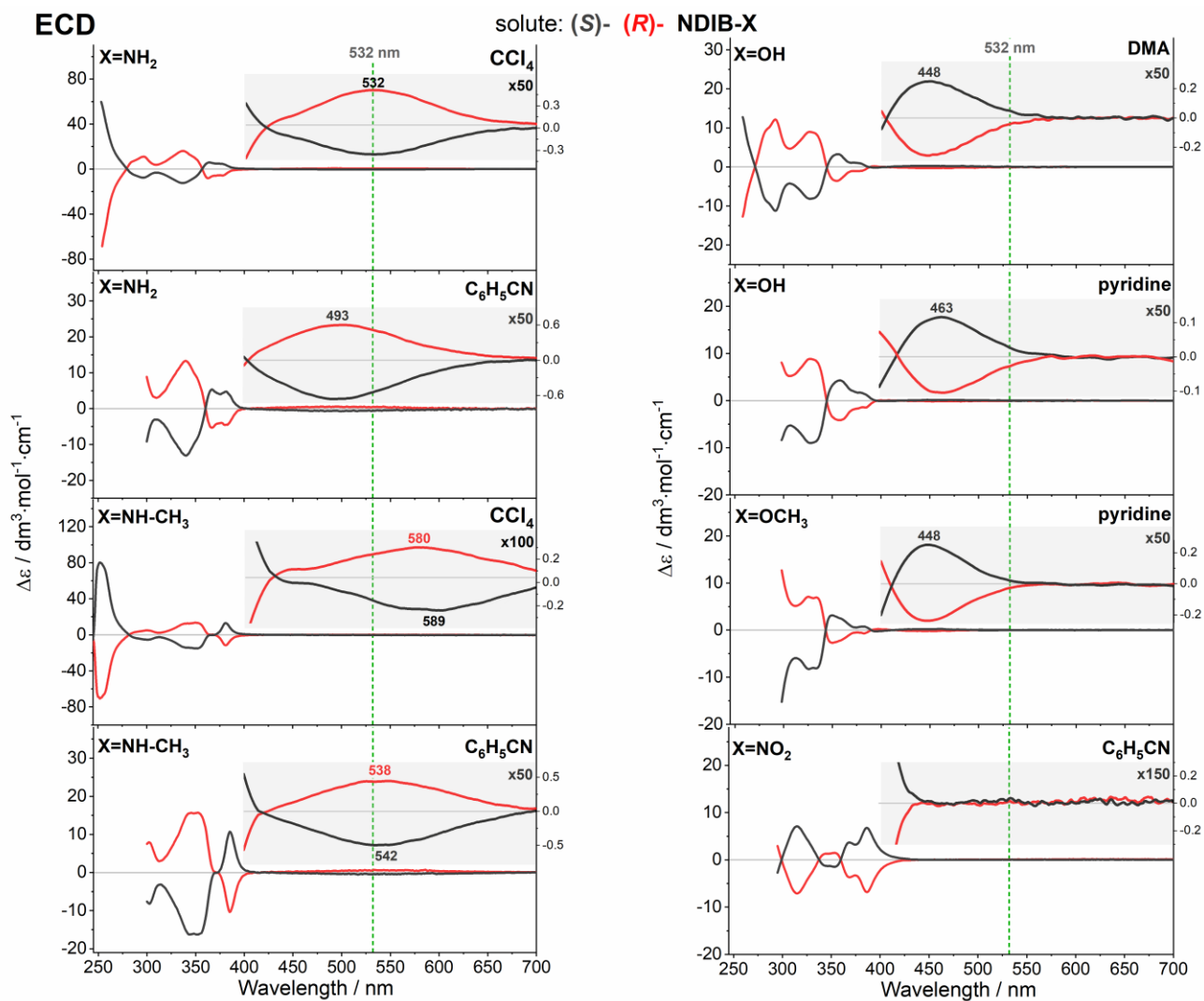


**Figure S9.** UV-Vis spectra of NDIB-X derivatives in  $\text{CHCl}_3$  and DMSO.



**Figure S10.** UV-Vis spectra of NDIB-X derivatives in CCl<sub>4</sub>, C<sub>6</sub>H<sub>5</sub>CN, pyridine and DMA.





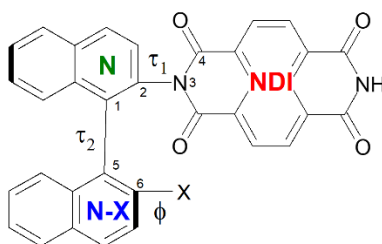
**Figure S11.** ECD spectra of NDIB-X derivatives in CCl<sub>4</sub>, C<sub>6</sub>H<sub>5</sub>CN, pyridine and DMA.

## 5. Explanation of the first ECD band sign by the DFT calculations

**Energy scan calculations** were performed for model (*S*)-NDIB-X systems, in which the H atom replaced the *n*Bu group (**Scheme S1**). During the unconstrained scans, the dihedral angle defining orientation of the X group with respect to the NDI ring ( $\phi$ ) was changed in 10° steps while the remaining geometrical parameters were relaxed. The angles between 0° and 180° correspond to the substituent directed outside the NDI—N-X cavity. In different molecules, different definitions of  $\phi$  dihedral angles to be changed were necessary (**Scheme S1**): C5-C6-O-H in NDIB-OH, C5-C6-O-C(H<sub>3</sub>) in NDIB-OCH<sub>3</sub>, C5-C6-N-H in NDIB-NH<sub>2</sub>, and C5-C6-N-H in NDI-NHCH<sub>3</sub>. Along with the unconstrained scans, the sign of the first ECD band was checked at each step and characteristic geometrical parameters:  $\tau_1$ (C4-C3-C2-C1),  $\tau_2$ (C2-C1-C5-C5) – describing the relative orientation of the N and NDI, N-X and N, and N-X and NDI rings, respectively. For X=NH<sub>2</sub> and NHCH<sub>3</sub> molecules the N atom inversion angle ( $\gamma_N$ ) was also checked.

One additional dihedral angle was frozen in the constrained scans: for the OH and OCH<sub>3</sub> derivatives it was the  $\tau_1$  angle fixed at c1 or c2 conformer geometry, i.e. at -80° or -110°. For NH<sub>2</sub> and NHCH<sub>3</sub> substituted molecules the N inversion angle,  $\gamma_N$ , was set at 30° or -30°. At each step, the sign of the first ECD band, as well as characteristic geometrical parameters, were checked.

In all calculations the CAM-B3LYP/D3/tzvp level<sup>5-8</sup> was used with the opt=modredundant option. The Gaussian 09 package<sup>11</sup> was applied for the quantum-chemical calculations and GaussView<sup>12</sup> for the visualization.



**Scheme S1** Main rings in NDIB-X molecules, where X stands for OH, OCH<sub>3</sub>, NH<sub>2</sub>, and NHCH<sub>3</sub> groups: naphthalenediimide (NDI), naphthalene (N), and substituted naphthalene (N-X). Atom numbering defining the  $\tau_1$ (C4-C3-C2-C1) and  $\tau_2$ (C2-C1-C5-C5) dihedral angles reflecting the relative twist of the NDI against N, as well as N against the N-X ring.  $\tau_1$  indicates the c1 and c2 conformation of the studied systems.  $\tau_2$  shows the twisting of the N against the N-X ring depending on their repulsion or attraction caused by the bulkiness of the substituent or the formation of the intramolecular hydrogen bonds between the C=O (NDI) and an X substituent.

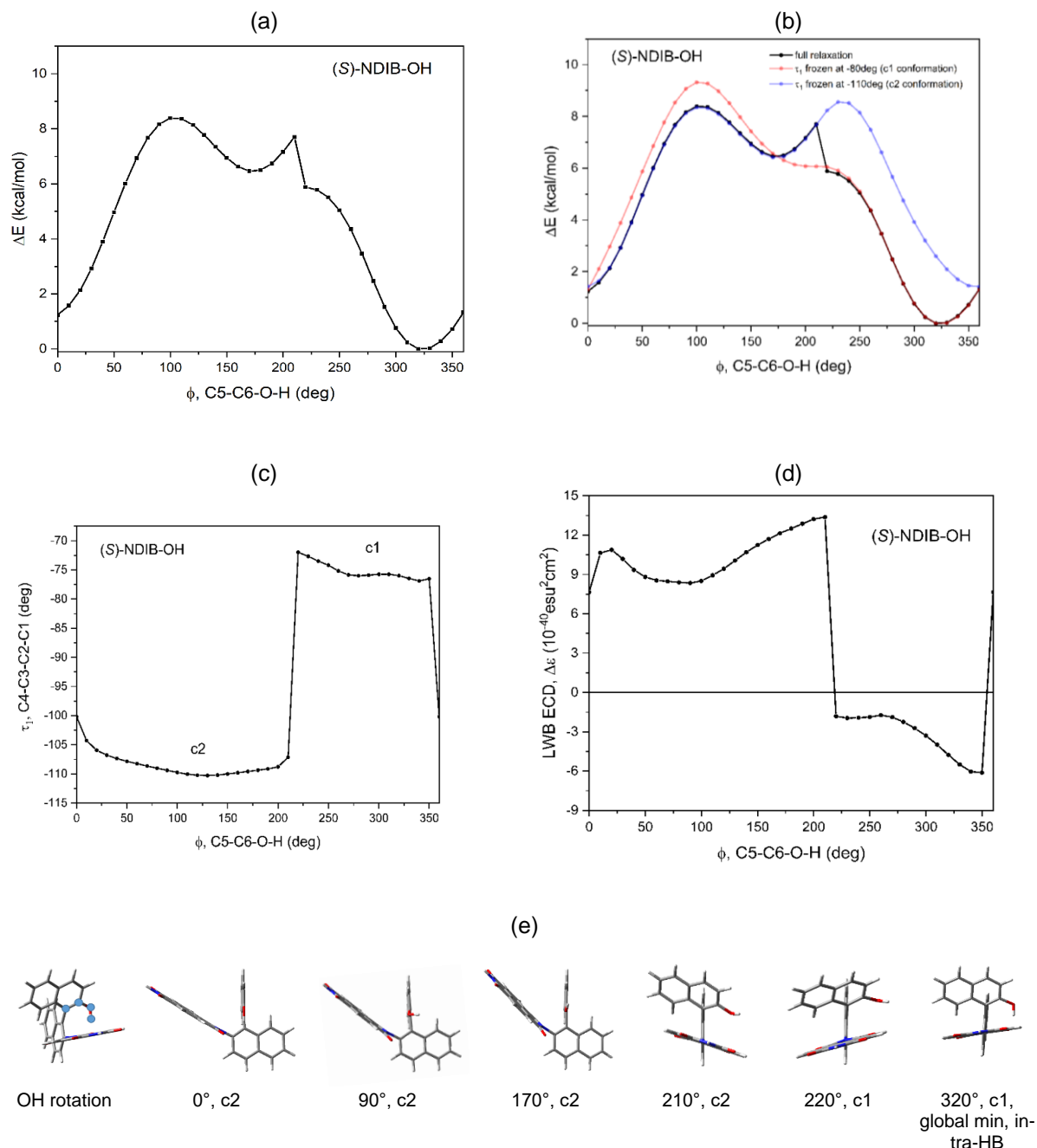
**(S)-NDIB-OH**: To understand why the signs of the first ECD band (and ECD-Raman) of the NDIB-OH in CHCl<sub>3</sub> and DMSO are different, we checked the energy and sign changes of the first ECD band with the rotation if the OH group performing the CAM-B3LYP/D3/TZVP calculations with unconstrained and some constrained parameters. The unconstrained energy scan (Figure S12a) shows discontinuity at ca. 220°. It is connected with a jump between the c1 and c2 conformers. Simply, for angles close to 180°, the potential curves corresponding to the two conformers (red and dark blue lines at Figure S12b) are crossing and on each side of the crossing point different conformer is energetically more stable. This can be clearly seen in the  $\tau_1$  changes on the OH rotation (Figure S12c).  $\tau_1$  defines the NDIB-OH conformers: it is around -75° and -110° for c1 and c2, respectively. The sign of the NDIB-OH first ECD band is directly related to the conformer present in the system: it is negative for c1 while positive for c2 (Figure S12d). Thus, rotation of the OH group enforces a change of conformation which entails a change of the first ECD band sign.

Notice that the (*S*)-NDIB-OH global minimum structure exhibits an intramolecular OH...O=C hydrogen-bond-like interaction (OH rotated to ca. -35°). For 0° < C5-C4-O-H < 180°, the OH group can be engaged in the intermolecular HB with a strong proton acceptor solvents such as DMSO, DMA, or pyridine. Note also that in the proton acceptor solvents the energy increase with the flip from the c1 to c2 conformer is compensated by an energy decrease due to hydrogen bonding with the solvent.

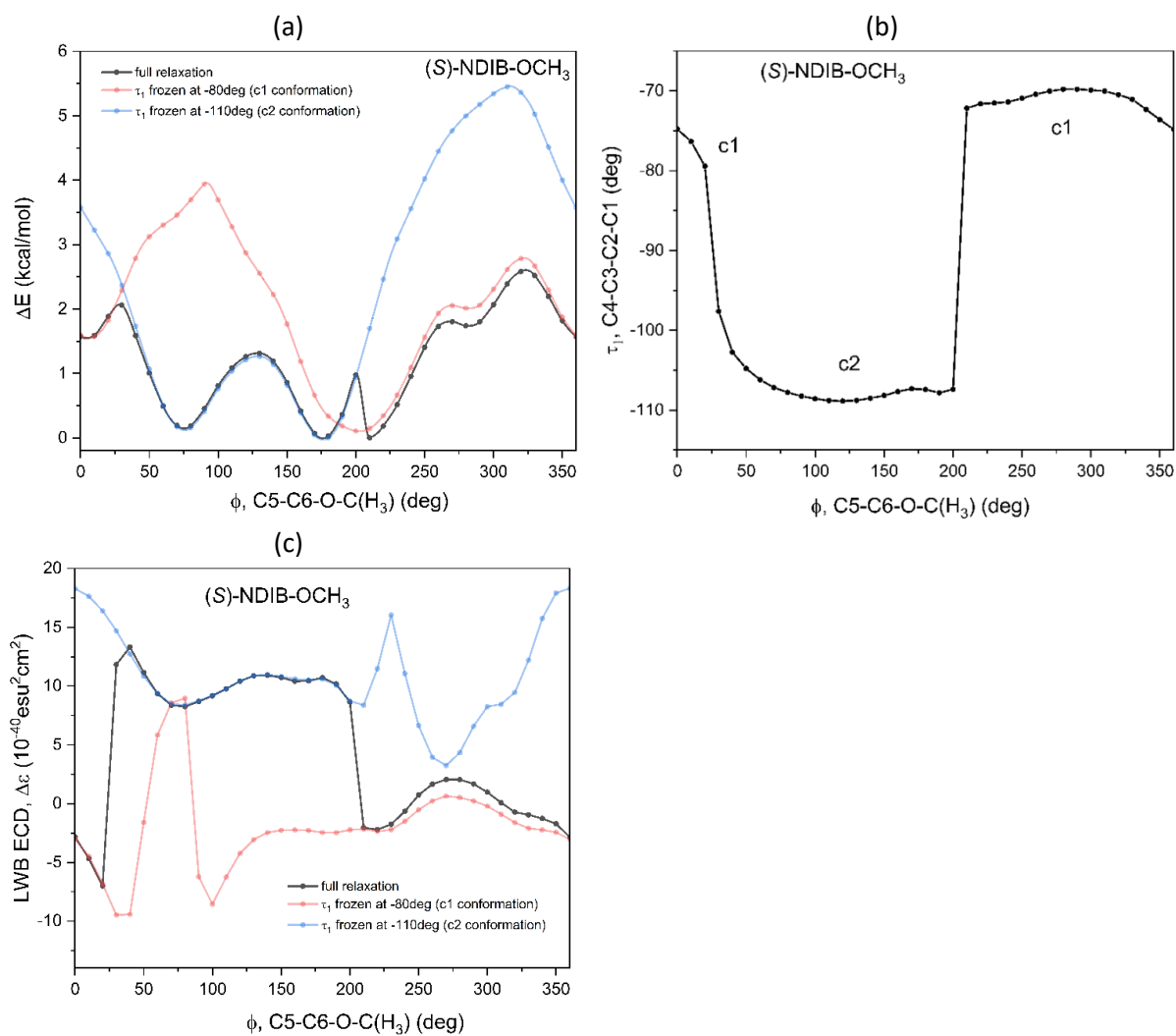
**(S)-NDIB-OCH<sub>3</sub>**: The experimental ECD spectrum of the OCH<sub>3</sub> derivative has already converted the sign of the first ECD band for CHCl<sub>3</sub> (Figure 3) and it remains converted in DMSO. This can be explained as for the OH substituent; however, the calculated profiles are more complex because more intramolecular interactions coexist for a slightly larger OCH<sub>3</sub> group. The energy profiles reveal that for the 30° < C5-C4-O-Me < 180° angles (defining the outward position of the methoxy group) only the c2 conformer can be present (Figure S13a). However, the other position of this group cannot be adopted because of the sterical repulsion. As for OH, this can be shown in the  $\tau_1$  changes on the OCH<sub>3</sub> rotation (Figure S13b), where again  $\tau_1$  defines the NDIB-OCH<sub>3</sub> conformers: it is around -70° and -105° for c1 and c2, respectively. Notice that greater complexity and non-monotonicity of the energy profiles (Figure S13a) indicate that more intramolecular interactions than simple OCH<sub>3</sub> rotation are involved. In conclusion, in the range of 30° < C5-C4-O-Me < 180° angles, which can only be adopted, only positive first ECD band signs are predicted (Figure S13c).

**(S)-NDIB-NH<sub>2</sub>**: The energy profile upon rotation of the substituent in the parent NDIB-NH<sub>2</sub> molecule would seem to have to be smooth. However, it is not so because of slight pyramidization of the NH<sub>2</sub> group. In the course of the NH<sub>2</sub> rotation (Figure S14a), the pyramid inversion occurs which is seen in the  $\gamma_N$  angle values ca.  $\pm 30^\circ$  (Figure S14b). Regardless the pyramid inversion, the first ECD band sign is constantly negative due to lack of conformational changes (Figures S14c and S14d).

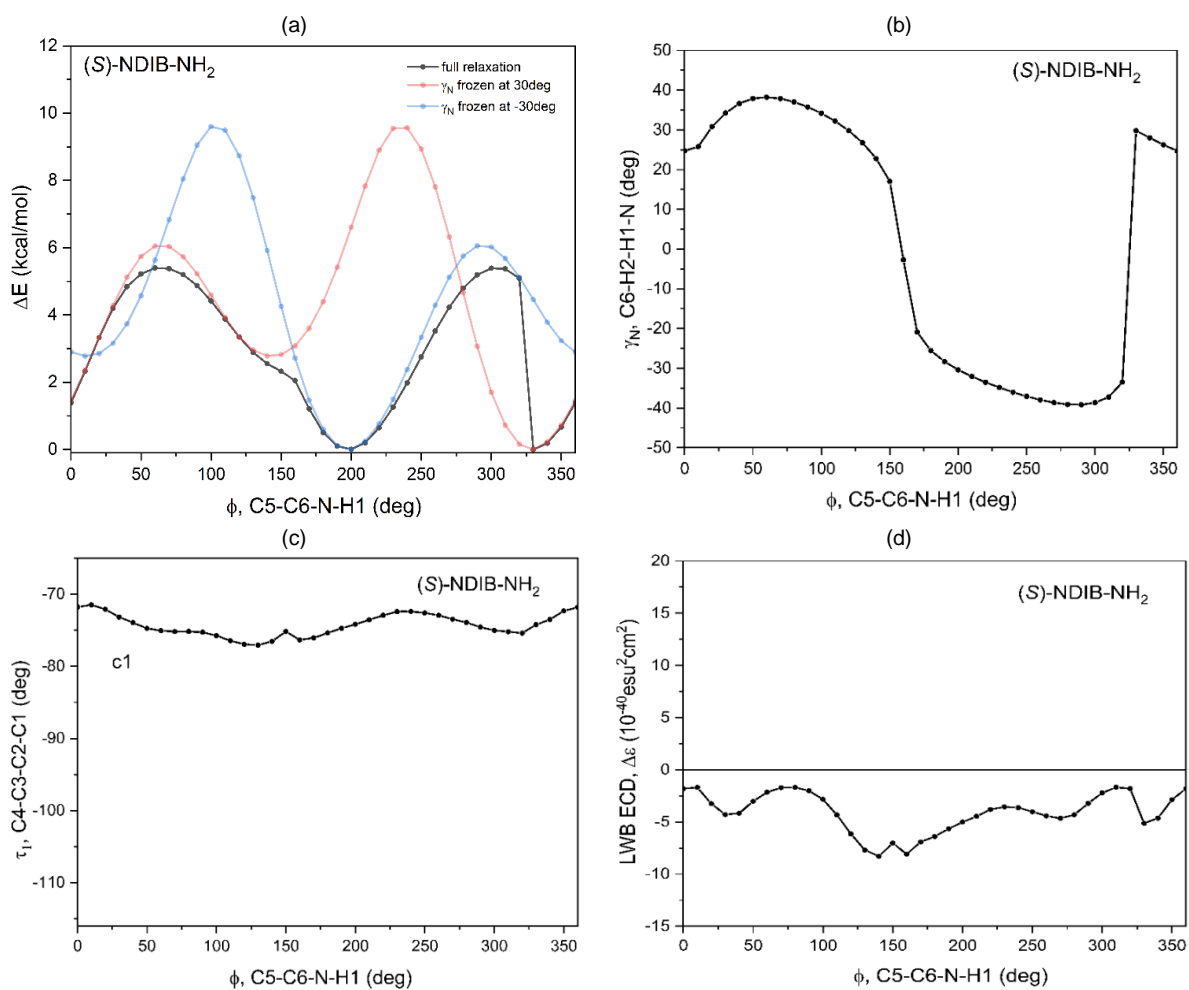
**(S)-NDIB-NHCH<sub>3</sub>**: Nevertheless, the energy and other parameter profiles for NDIB-NHCH<sub>3</sub> appear more complex (Figure S15), and can be interpreted in full analogy to the changes noticed for the NH<sub>2</sub> substituent. The only important characteristics in the profiles are connected to the  $\gamma_N$  angle value changes.



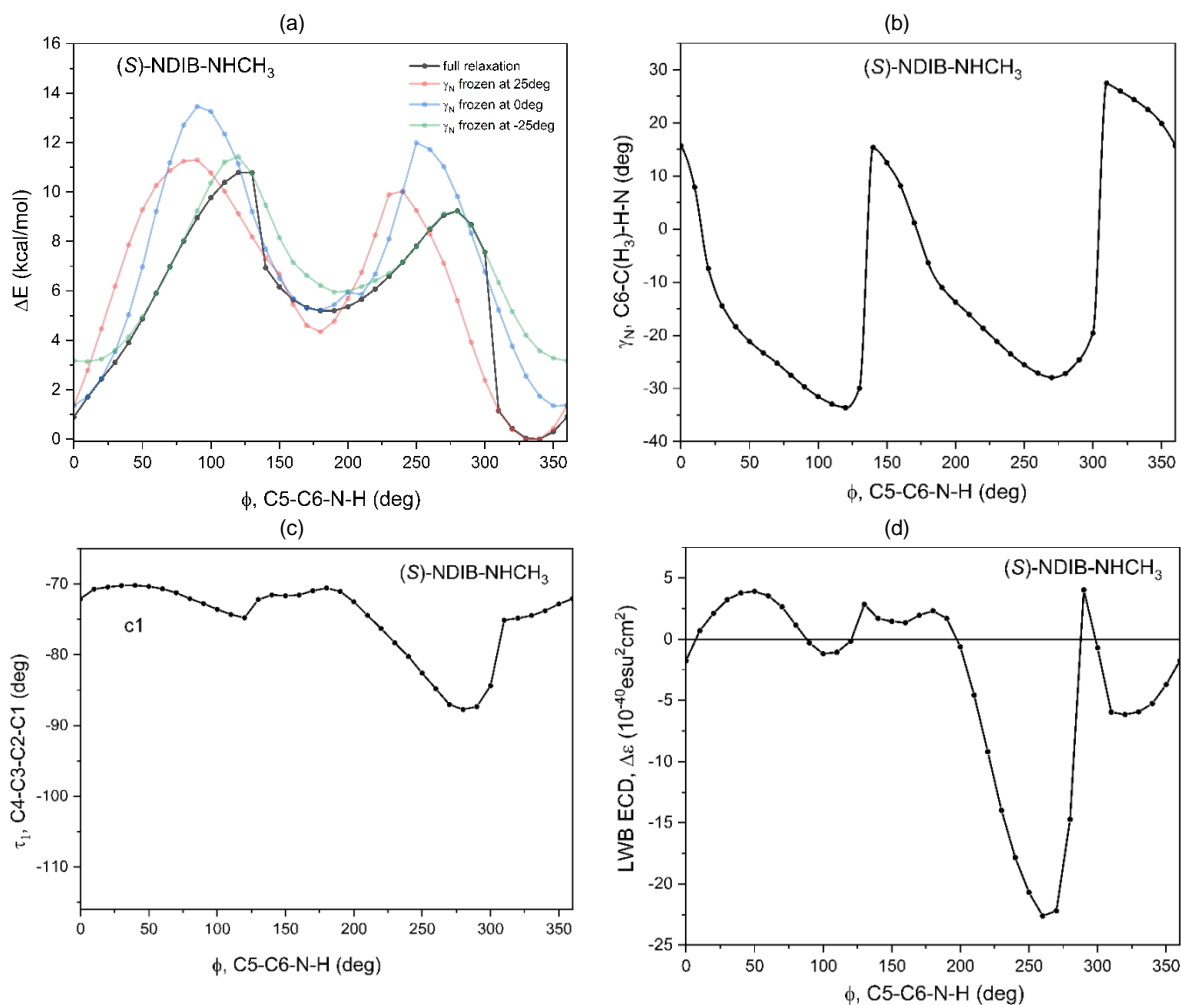
**Figure S12.** The CAM-B3LYP/D3/TZVP estimated energy of (a) the unconstrained (black) and (b) the  $\tau_1$  constrained rotations (red and blue) as well as (c) the  $\tau_1$ (C4-C3-C2-C1) and (d) sign of the first ECD band change with the OH group rotation in (S)-NDIB-OH derivative. Conformers c1 and c2 are marked in red and blue, respectively. (e) The (S)-NDIB-OH geometries important for the presented curves: the global minimum structure exhibits intramolecular OH...O=C hydrogen-bond-like interaction. For  $0^\circ < \text{C5-C4-O-H} < -180^\circ$ , the OH group can be engaged in the intermolecular HB with a strong proton acceptor solvent such as DMSO, DMA, or pyridine. Notice that in proton acceptor solvents the energy increase with the flip from the c1 to c2 conformer is compensated by energy decrease due to hydrogen bonding with the solvent.



**Figure S13.** The CAM-B3LYP/D3/TZVP estimated energies (a) of the unconstrained (black) and the  $\tau_1$  constrained rotations (red and blue) as well as (b) the  $\tau_1$ (C4-C3-C2-C1) and (c) sign of the first ECD band change with the OCH<sub>3</sub> group rotation in (S)-NDIB-OCH<sub>3</sub> derivative. Conformers c1 and c2 are marked in red and blue, respectively. Greater complexity and non-monotonicity of the profiles indicate that more intramolecular interactions than simple OCH<sub>3</sub> rotation are involved.



**Figure S14.** The CAM-B3LYP/D3/TZVP estimated energies (a) of the unconstrained (black) and the  $\nu_N$  constrained rotations (red and blue) as well as (b) the  $\nu_N$  nitrogen inversion, (c)  $\tau_1$ (C4-C3-C2-C1), and (d) sign of the first ECD band change with the NH<sub>2</sub> group rotation in (S)-NDIB-NH<sub>2</sub> derivative. The discontinuities present in the energy profiles due to rotation of the NH<sub>2</sub> group are caused by the amine group inversion when the C6-H1-H2-N dihedral angle was unconstrained. Notice, that during the NH<sub>2</sub> group rotation (black line) the conformation of the (S)-enantiomer is always c1 entailing positive value of rotational strength. Notice that the (S)-NDIB-NH<sub>2</sub> global minimum exhibits an intramolecular NH $\cdots$ O=C hydrogen-bond-like interaction. There are two equivalent minima: one of them corresponds to the HB interaction with one of the H atoms of the NH<sub>2</sub> group whereas the other with the second one.



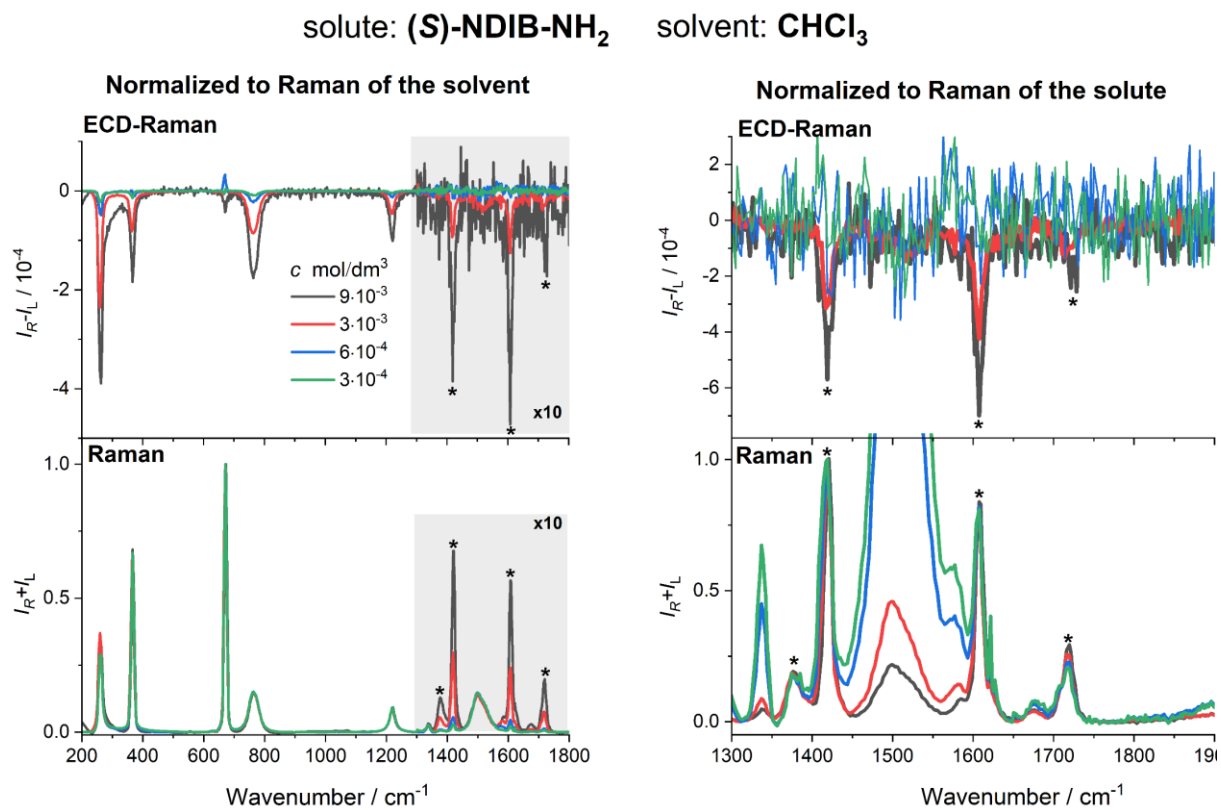
**Figure S15.** The CAM-B3LYP/D3/TZVP estimated energies (a) of the unconstrained (black) and the  $v_N$  constrained rotations (red, green, and blue) as well as (b) the  $v_N$  nitrogen inversion, (c)  $\tau_1$ (C4-C3-C2-C1), and (d) sign of the first ECD band change with the NHCH<sub>3</sub> group rotation in the (S)-NDIB-NHCH<sub>3</sub> derivative. The discontinuities present in the energy profiles due to rotation of the NHCH<sub>3</sub> group are caused by the NHCH<sub>3</sub> group inversion at the N-atom when the C6-H1-H2-N dihedral angle was unconstrained. Notice, that during the NHCH<sub>3</sub> group rotation (black line) conformation of the (S)-enantiomer is always c1, however, the rotational strength is positive or negative indicating more complex intramolecular interactions during NHCH<sub>3</sub> rotation. In the most stable arrangement, the intramolecular NH...O=C hydrogen-bond-like interaction is present.

## 6. The Raman and ROA measurements

Raman and ROA spectra of NDI-derivatives in solvents, i.e.,  $\text{CHCl}_3$ ,  $\text{CCl}_4$ ,  $\text{C}_6\text{H}_5\text{CN}$ , DMSO, pyridine and DMA were measured using a ChiralRAMAN-2X<sup>TM</sup> spectrometer (BioTools Inc.) at a resolution of  $7\text{ cm}^{-1}$  in the range of  $2500\text{--}180\text{ cm}^{-1}$  employing the excitation wavelength of 532 nm. The solutions of NDI-derivatives (ca.  $c=3\times 10^{-3}\text{ mol/dm}^3$ ) were measured in ROA quartz optical cells with anti-reflective coating. Additionally, for the NDIB- $\text{NH}_2$  in  $\text{CHCl}_3$  three other molar concentrations were studied ( $9\times 10^{-3}$ ,  $6\times 10^{-4}$  and  $3\times 10^{-4}$ ) to check how different concentrations influence intensity of the ECD-Raman effect, both of the solvent and solute, and to find out whether it is possible to minimize the ECD-Raman effect to the point where true RROA can be observed. Before measurements, the NDI-derivatives solutions were purified by using the activated charcoal and then they were filtered with Millipore<sup>TM</sup> Millex<sup>®</sup> syringe filters (pore size  $0.45\text{ }\mu\text{m}$ ) to eliminate chemical impurities. The Raman and ROA spectra were collected in 2 s of integration time. Other experimental conditions such as laser power and data collection time were matched for each sample individually (**Table S4**). The baseline of Raman and ROA spectra were subtracted by the asymmetric least squares smoothing method. Then the ROA spectra were smoothed with the ten-point Savitzky–Golay procedure using OriginPro software.

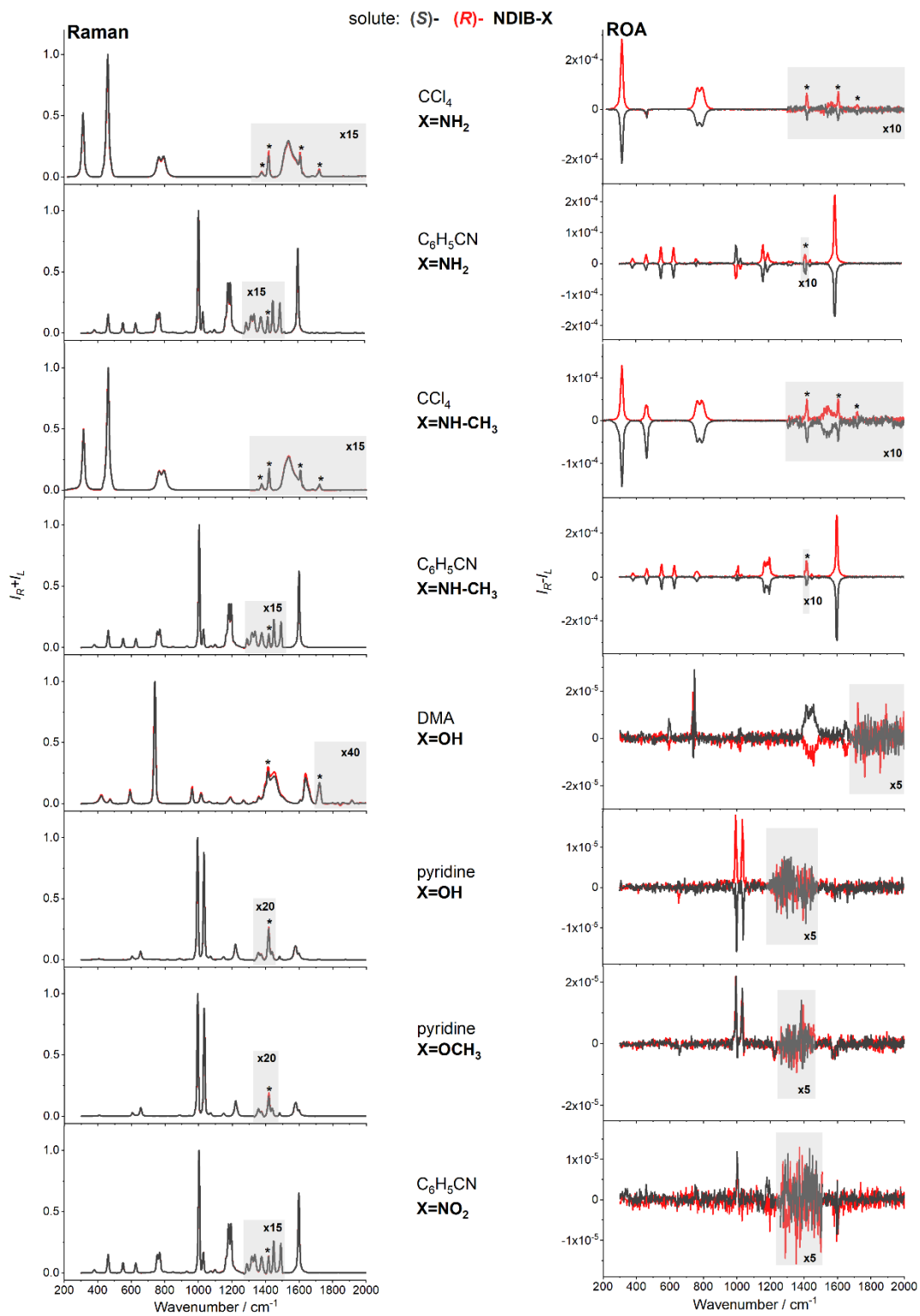
**Table S4.** Raman and ROA measurement parameters for solutions of the NDIB-X derivatives.

X	Solvent	Power of laser (mW)		Data collection time (h)	
		(S)	(R)	(S)	(R)
NH <sub>2</sub>	CHCl <sub>3</sub>	140	140	48	48
	CCl <sub>4</sub>	160	160	24	24
	DMSO	60	60	24	24
	C <sub>6</sub> H <sub>5</sub> CN	50	50	24	24
NH-CH <sub>3</sub>	CHCl <sub>3</sub>	150	130	27	27
	CCl <sub>4</sub>	42	42	39	42
	DMSO	42	42	38	29
	C <sub>6</sub> H <sub>5</sub> CN	34	34	24	24
OH	CHCl <sub>3</sub>	94	100	24	24
	DMSO	34	34	24	24
	pyridine	30	30	60	42
	DMA	70	100	46	36
OCH <sub>3</sub>	CHCl <sub>3</sub>	90	100	36	35
	DMSO	70	70	24	24
	pyridine	30	30	34	35
NO <sub>2</sub>	CHCl <sub>3</sub>	66	66	24	24
	DMSO	90	90	24	32
	C <sub>6</sub> H <sub>5</sub> CN	26	24	25	27



**Figure S16.** Experimental Raman and ROA (ECD-Raman) spectra of (S)-NDIB-NH<sub>2</sub> in CHCl<sub>3</sub> at different molar concentrations. Right panel: spectra normalized to maximum Raman intensity of the solvent, left panel: spectra normalized to maximum Raman intensity of the solute; for both cases CID ratios (ROA/Raman) are preserved.





**Figure S17.** Experimental Raman and ROA spectra of NDIB-derivatives in CCl<sub>4</sub>, C<sub>6</sub>H<sub>5</sub>CN, pyridine and DMA.

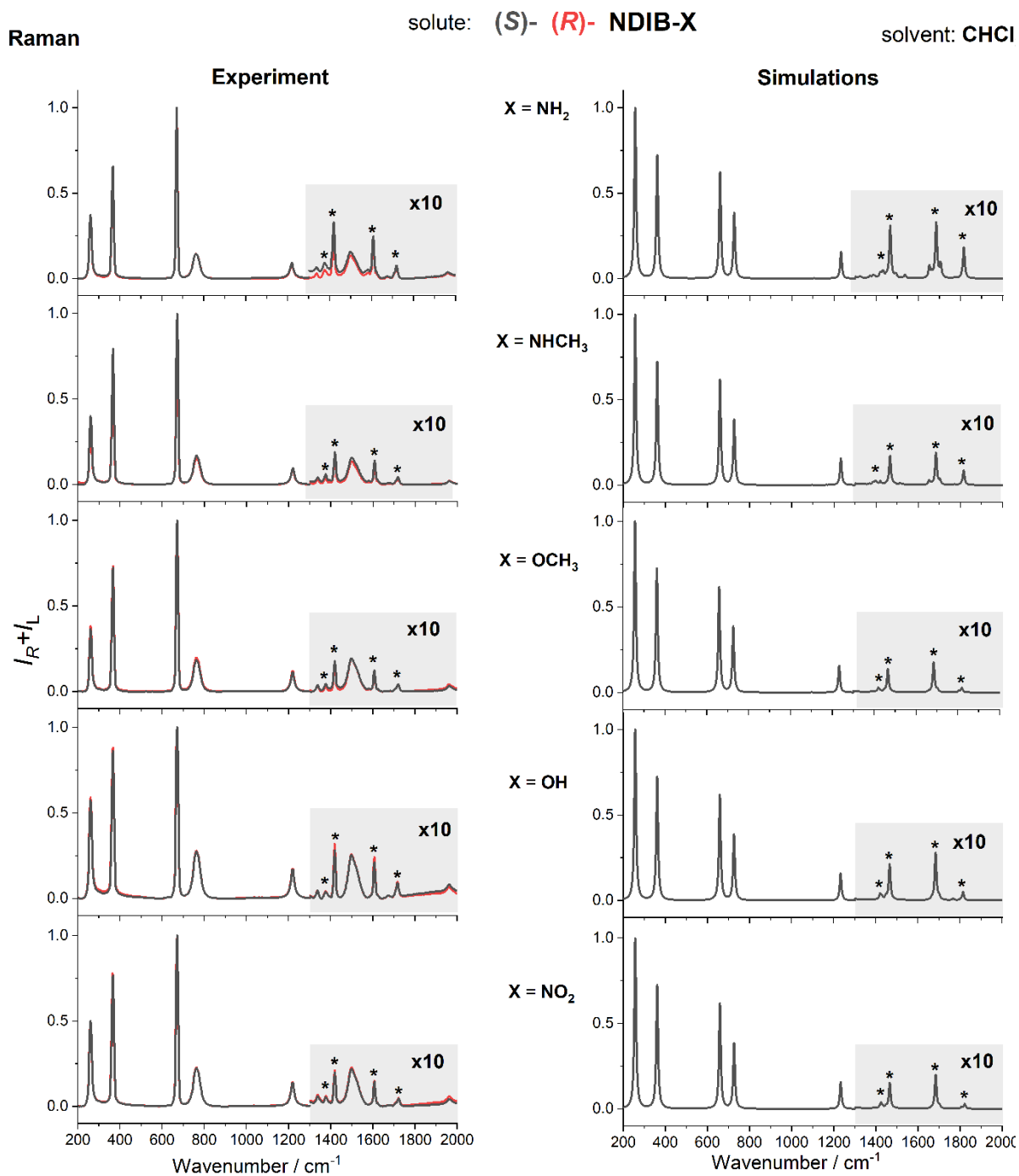
## 6. Simulations of the Raman, ROA, and ECD-Raman spectra

The Raman spectra of NDIB-X solutes, and selected solvents, were calculated in Gaussian G16.C01 software, at the CAM-B3LYP/TZVP theory level, using the 480 nm excitation line, which best represents the position of the experimental (532 nm) laser line with respect to the position of the experimental first ECD band. The theoretical laser line is hypsochromically shifted with respect to the experimental one by the same value in  $\text{cm}^{-1}$  as the position of the CT band maximum from the calculations relative to the experiment. The ECD-Raman spectra were calculated separately for NDIB-X solutes and solvents, accordingly to the Eq. 1, in use of experimental  $\Delta\varepsilon$ ,  $\Delta\varepsilon'$  and  $c$ , theoretical *DOC* factors and Raman/ROA intensities, as well as  $L$  and  $L'$  equal to 2 mm and 1 mm respectively. Appropriate ECD-Raman (and Raman) spectra of the NDIB-X solutes and solvents were summed using scaling factors obtained from the experimental spectra, to get similar ratio of the solutes and solvents band intensities as in the experiment. To enable the comparison of the theoretical and experimental spectra, and to compare the calculated ECD-Raman and ROA spectra, the calculated ECD-Raman spectra were normalized with the Raman spectra, preserving the CID ratios.

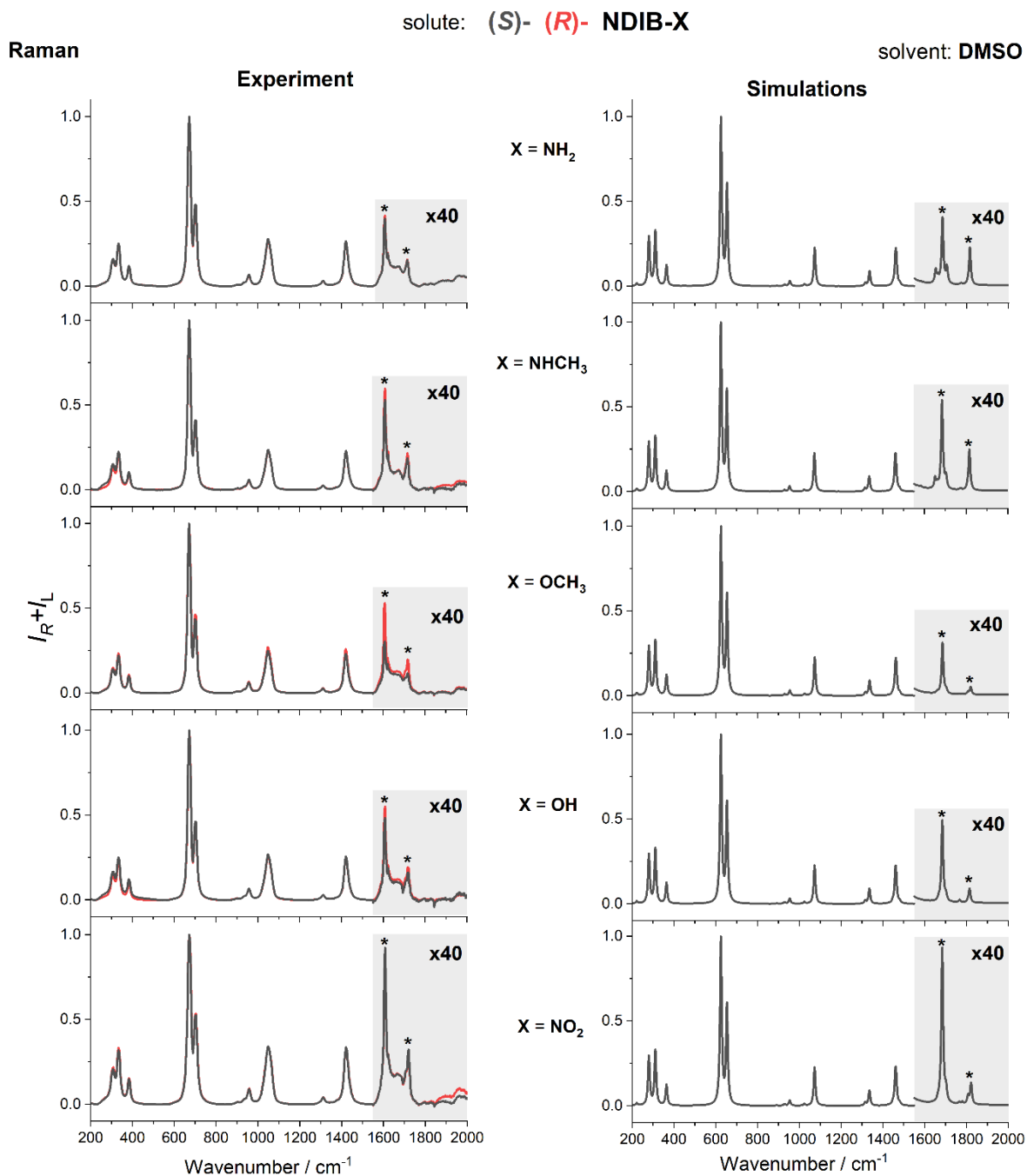
Influence of the wavelength of the excitation line on the calculated Raman and ROA spectra of all (*S*)-NDIB-X analogues was also done.

The main reason for the simulations at various Raman excitation wavelengths was to check whether the experimental ROA signals are indeed due to the ECD-Raman effect, or due to true, natural RROA. It was not clear whether the main contribution to the possible true RROA has the resonance with the weak 1<sup>st</sup> electronic transition (with negative ECD for (*S*)-NDIB-NH<sub>2</sub>) that is energetically matched energetically with the excitation line or rather the resonance with much stronger 2<sup>nd</sup> transition (with positive ECD for (*S*)-NDIB-NH<sub>2</sub>). If the 2<sup>nd</sup> transition contributes to the resonance more, and the calculated ROA is negative at the 480 nm line, the monosigned, negative ROA signal of the solute for (*S*)-NDIB-NH<sub>2</sub> could be interpreted as a true RROA. However, calculations have shown that eg. for the (*S*)-NDIB-NH<sub>2</sub> the resonance due to the 1<sup>st</sup> transition dominates for all used excitation lines around 480 nm  $\pm$  100 nm. Furthermore, to get opposite (positive) signed ROA, much lower wavelengths need to be used (below 360 nm). There are two possibilities to for representing the ROA intensities, either normalized with Raman or without such a normalization. The normalization with Raman provides the opportunity to compare the calculated ROA intensity with the ECD-Raman one which shows that the intensity of the calculated ROA is generally too high. In consequence, in the summed natural ROA with ECD-Raman (as for vitamin B<sub>12</sub> in Ref. 15), in contradiction to the experimental findings, the sign of the bands disagrees with the experiment and, in each case, instead of the ECD-Raman the natural ROA is dominating. On the other hand, skipping the normalization provides relative intensity differences in the Raman and ROA spectra at different wavelengths.

Two sets of figures with both normalization options are shown below. They also show that, assuming that the ECD-Raman effect does not exist, to obtain the sign of the natural ROA bands, as in the experiment, one should use a much shorter wavelength laser line to energetically approach the next electron transitions with respect to the CT one.

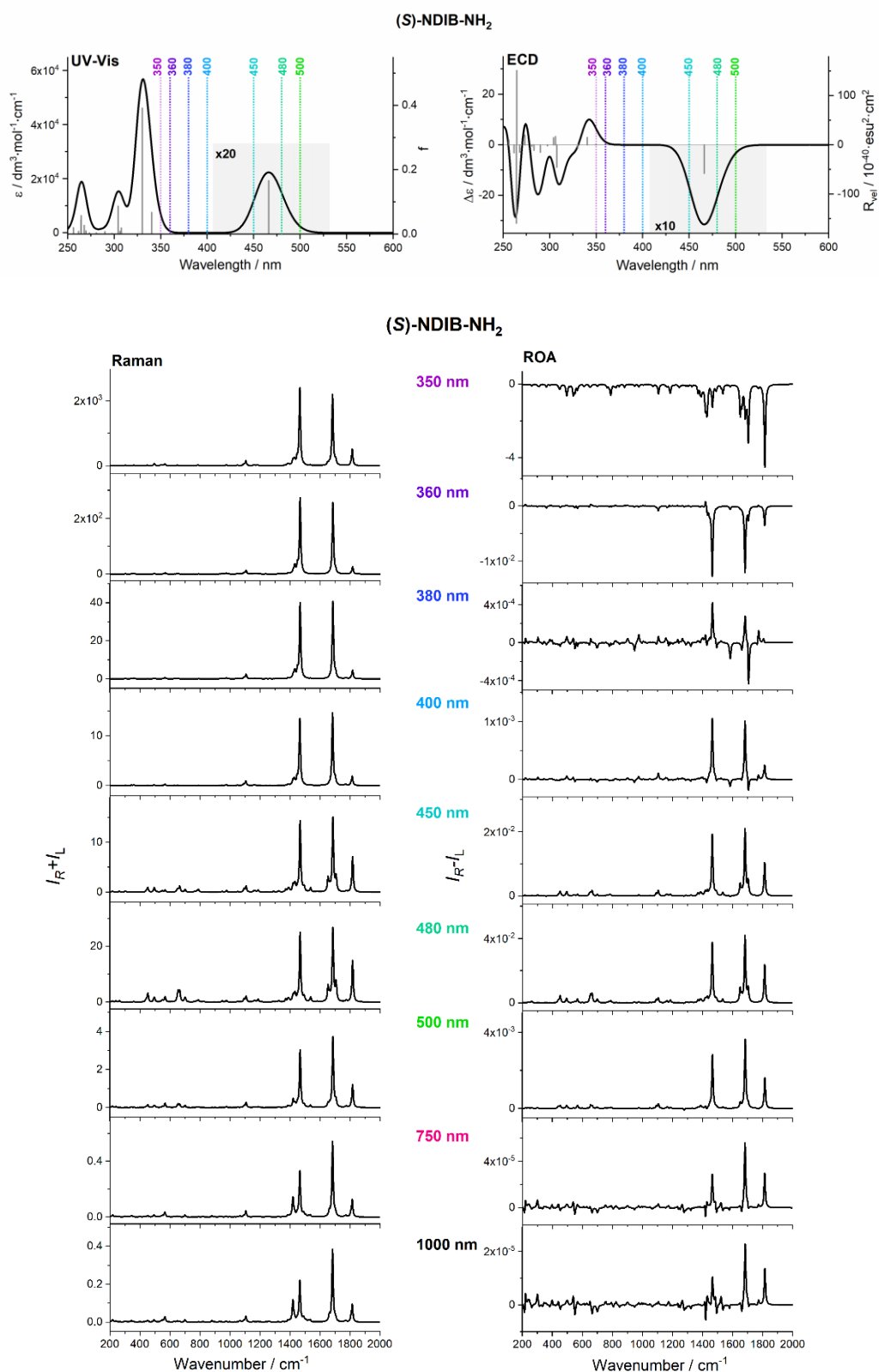


**Figure S18.** Comparison of the experimental (left) and simulated (right) Raman spectra of the NDIB-derivatives in chloroform. The Raman spectra are calculated as a superposition of the spectra simulated for the solvent and NDIB-derivatives separately.

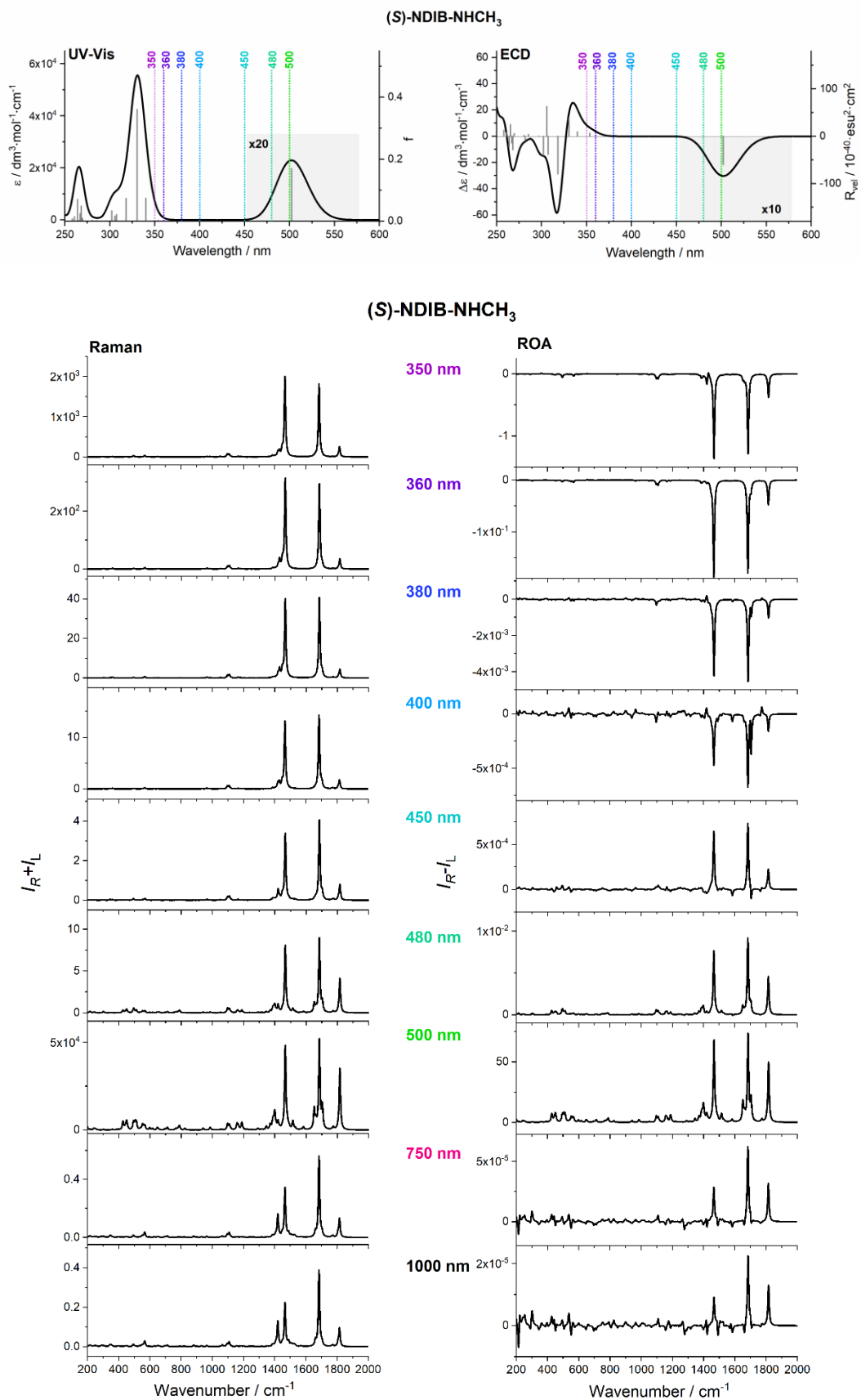


**Figure S19.** Comparison of the experimental (left) and simulated (right) Raman spectra of the NDIB-derivatives in DMSOs. The Raman spectra are calculated as a superposition of the spectra simulated for the solvent and NDIB-derivatives separately.

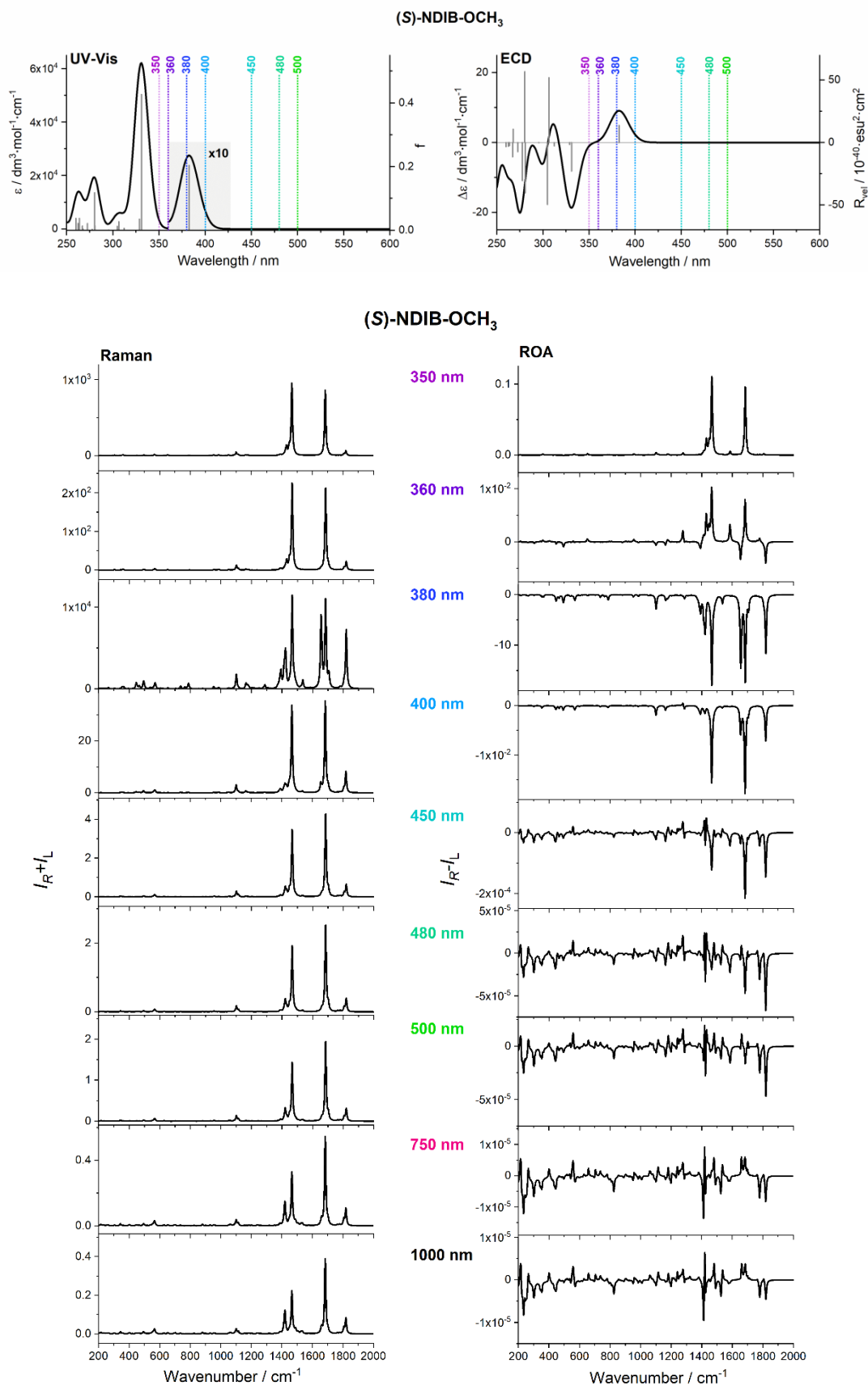
## The ROA intensities are not normalized with Raman



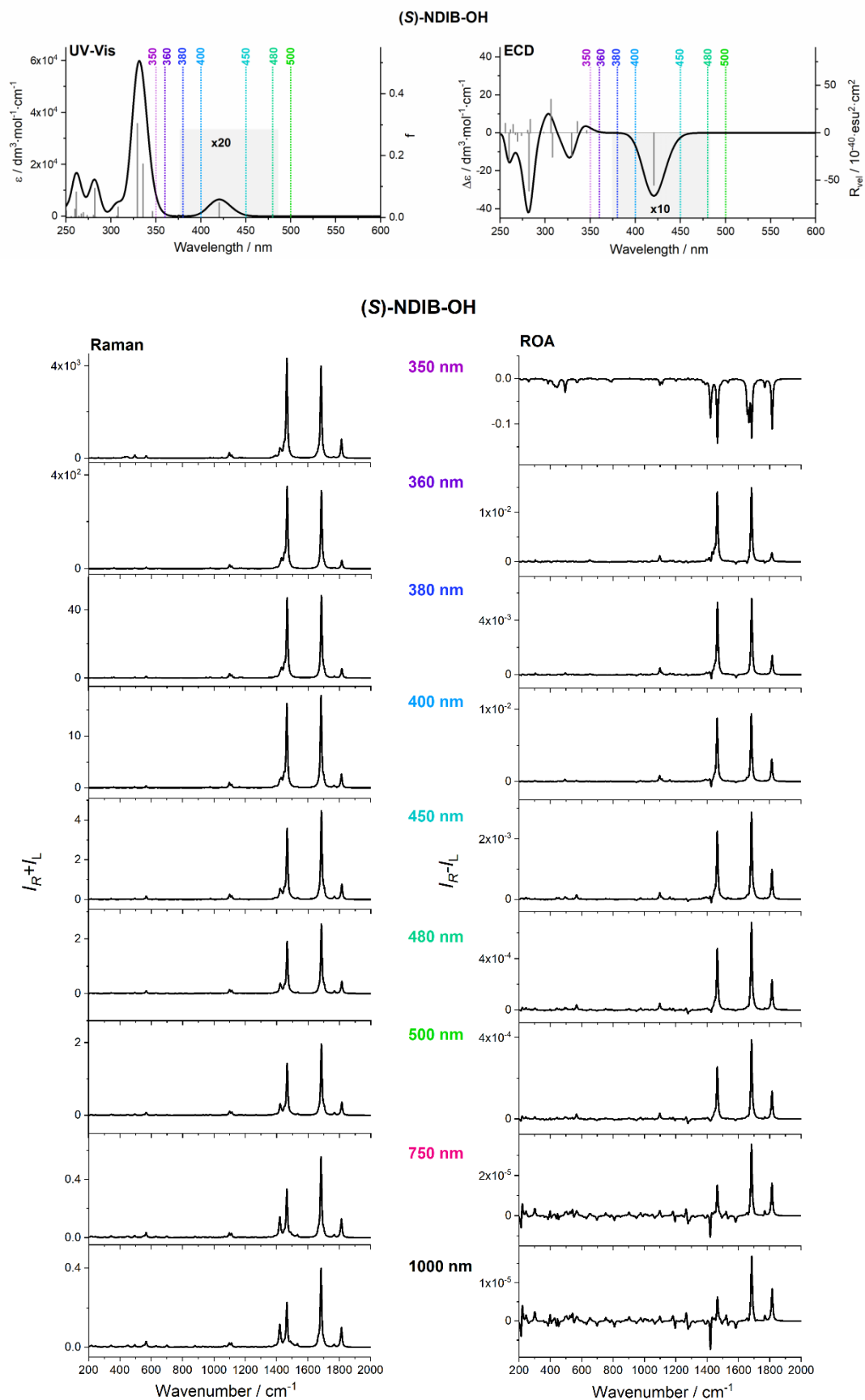
**Figure S20.** (Top) The CAM-B3LYP/ TZVP calculated UV (left) and ECD (right) spectra of (S)-NDIB-NH<sub>2</sub>. (bottom) The CAM-B3LYP/ TZVP calculated Raman (left) and ROA (right) spectra of NDIB-NH<sub>2</sub> by using different excitation lines. The ROA intensities are not normalized to the Raman ones. Calculations were performed using *Gaussian 16* suit of programs.<sup>16</sup>



**Figure S21.** (Top) The CAM-B3LYP/ TZVP calculated UV (left) and ECD (right) spectra of (S)-NDIB- NHCH<sub>3</sub>. (bottom) The CAM-B3LYP/ TZVP calculated Raman (left) and ROA (right) spectra of NDIB-NHCH<sub>3</sub> by using different excitation lines. The ROA intensities are not normalized to the Raman ones. Calculations were performed by using Gaussian 16 suit of programs.

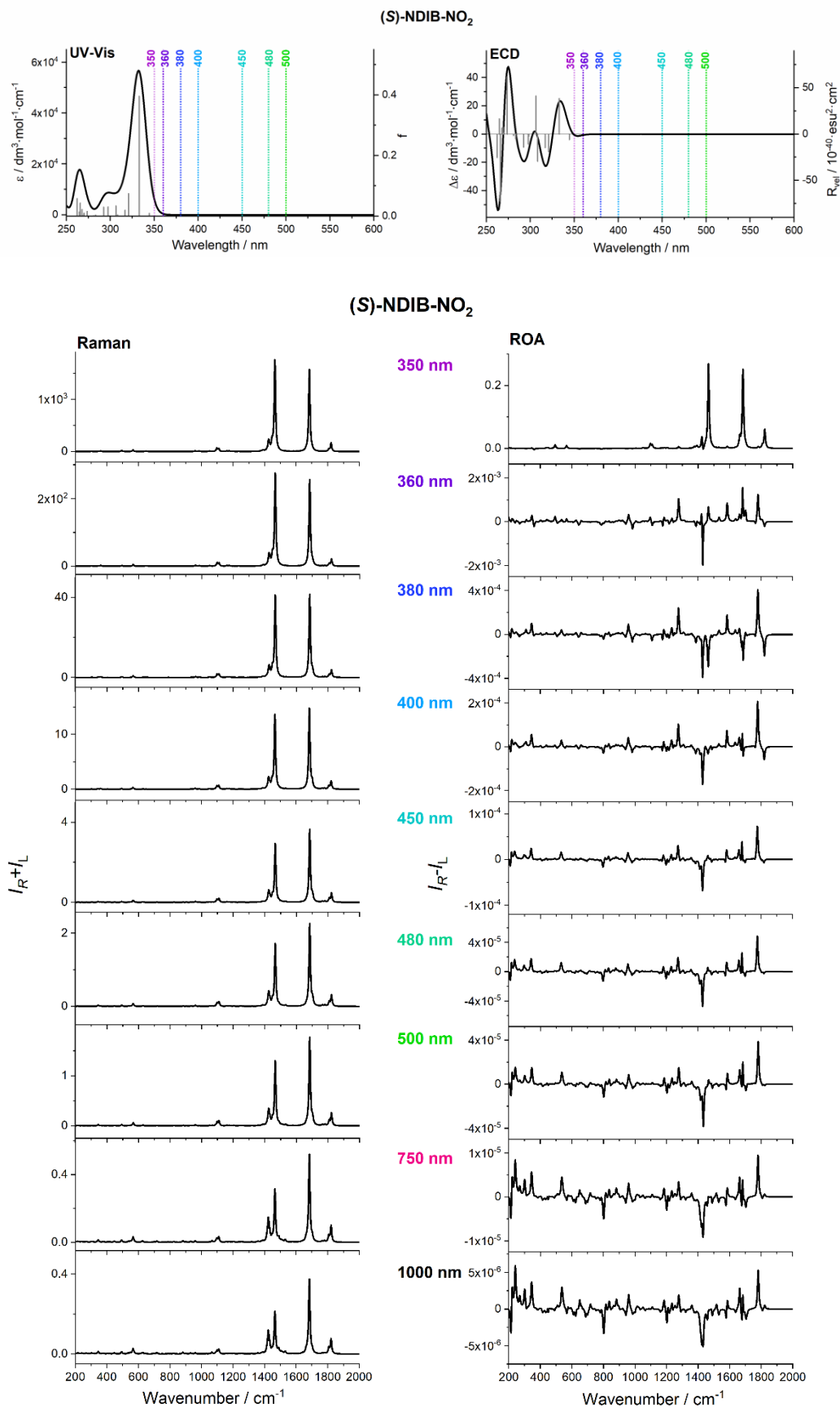


**Figure S22.** (Top) The CAM-B3LYP/ TZVP calculated UV (left) and ECD (right) spectra of (S)-NDIB-OCH<sub>3</sub>. (bottom) The CAM-B3LYP/ TZVP calculated Raman (left) and ROA (right) spectra of NDIB-OCH<sub>3</sub> by using different excitation lines. The ROA intensities are not normalized to the Raman ones. Calculations were performed by using Gaussian 16 suit of programs.



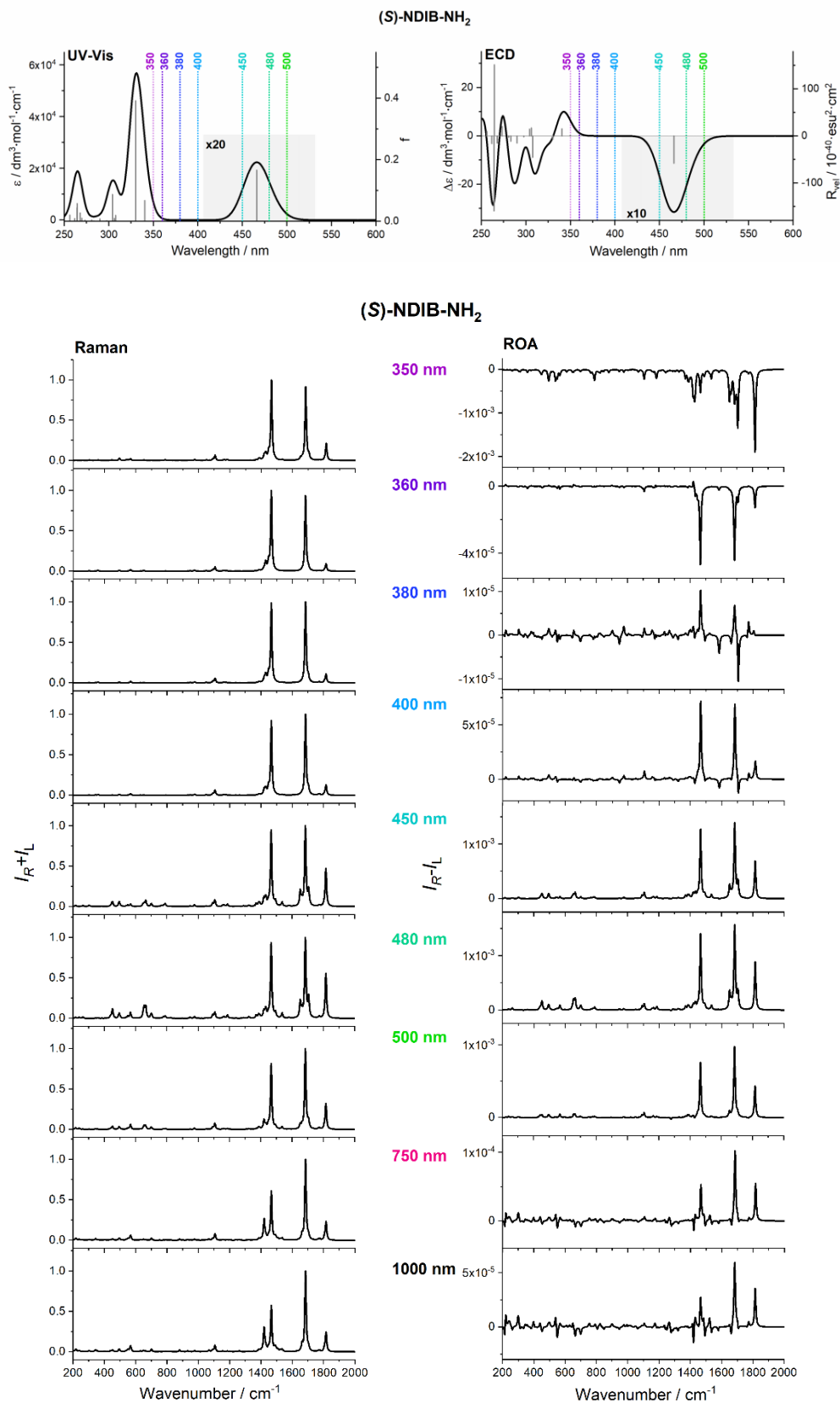
**Figure S23.** (Top) The CAM-B3LYP/ TZVP calculated UV (left) and ECD (right) spectra of (S)-NDIB-OH. (bottom) The CAM-B3LYP/ TZVP calculated Raman (left) and ROA (right) spectra of NDIB-OH by using different excitation lines. The ROA intensities are not normalized to the Raman ones. Calculations were performed by using Gaussian 16 suit of programs.



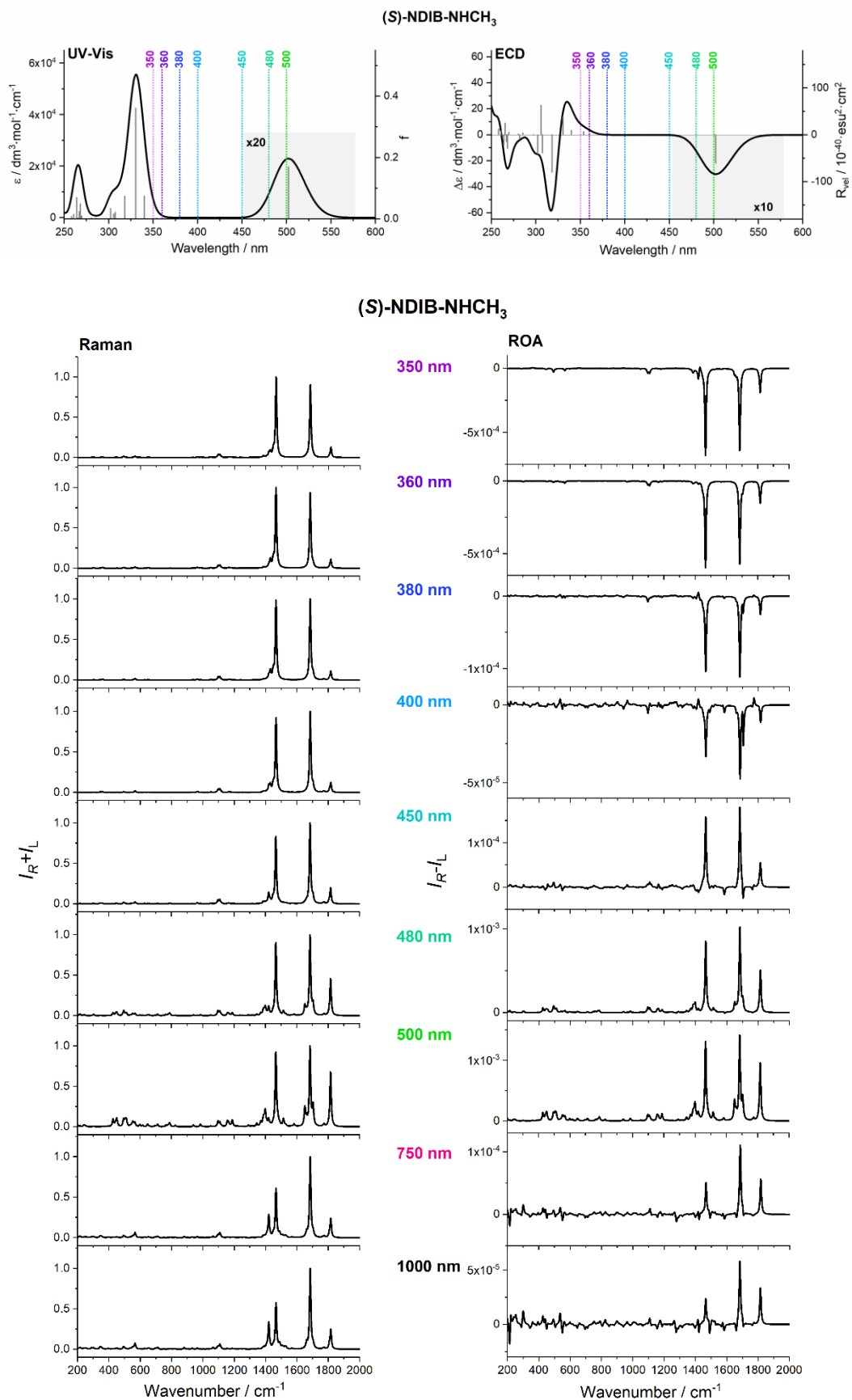


**Figure S24.** (Top) The CAM-B3LYP/ TZVP calculated UV (left) and ECD (right) spectra of (S)-NDIB-NO<sub>2</sub>. (bottom) The CAM-B3LYP/ TZVP calculated Raman (left) and ROA (right) spectra of NDIB-NO<sub>2</sub> by using different excitation lines. The ROA intensities are not normalized to the Raman ones. Calculations were performed by using Gaussian 16 suit of programs.

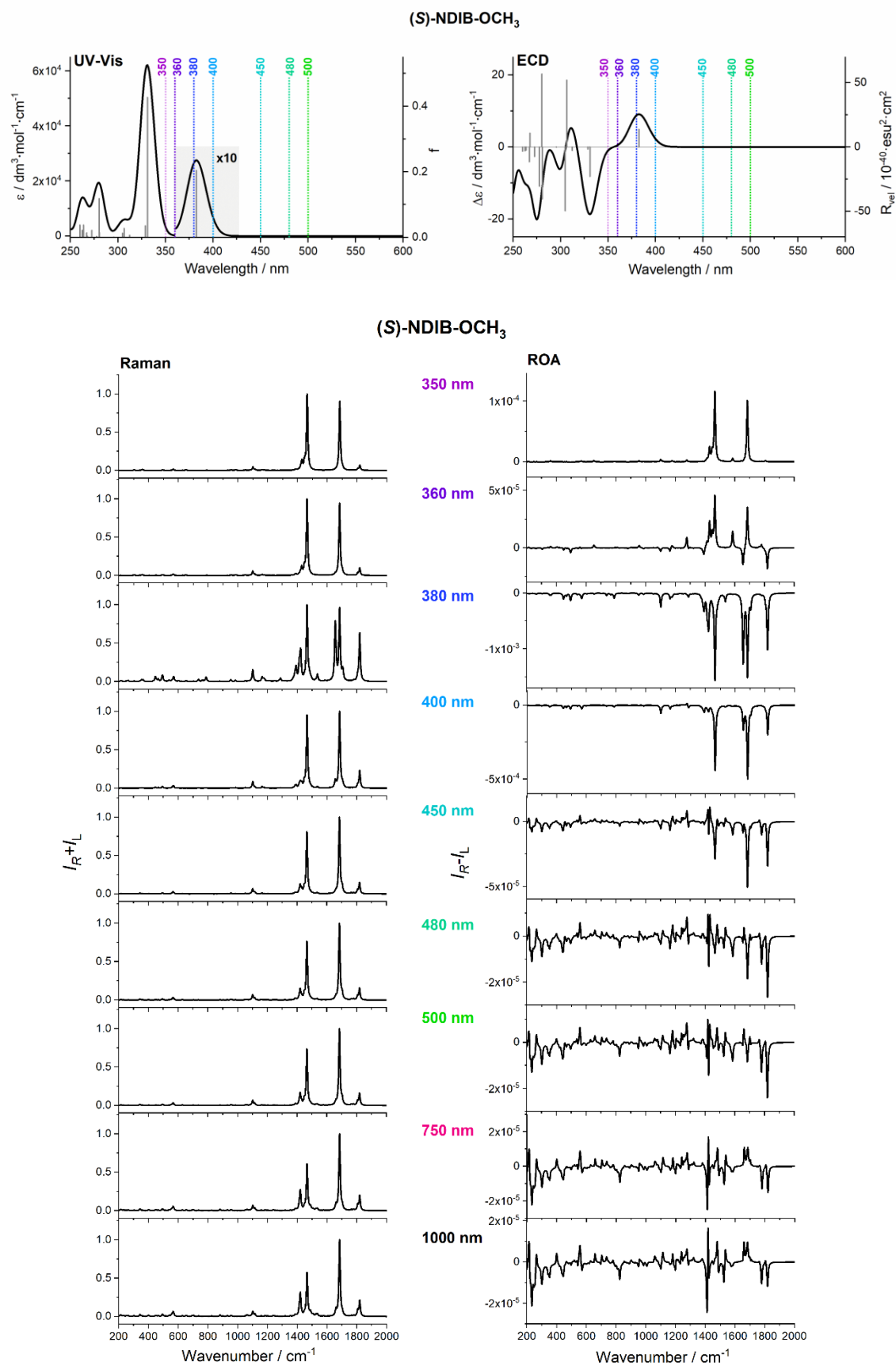
## The ROA intensities are normalized with Raman



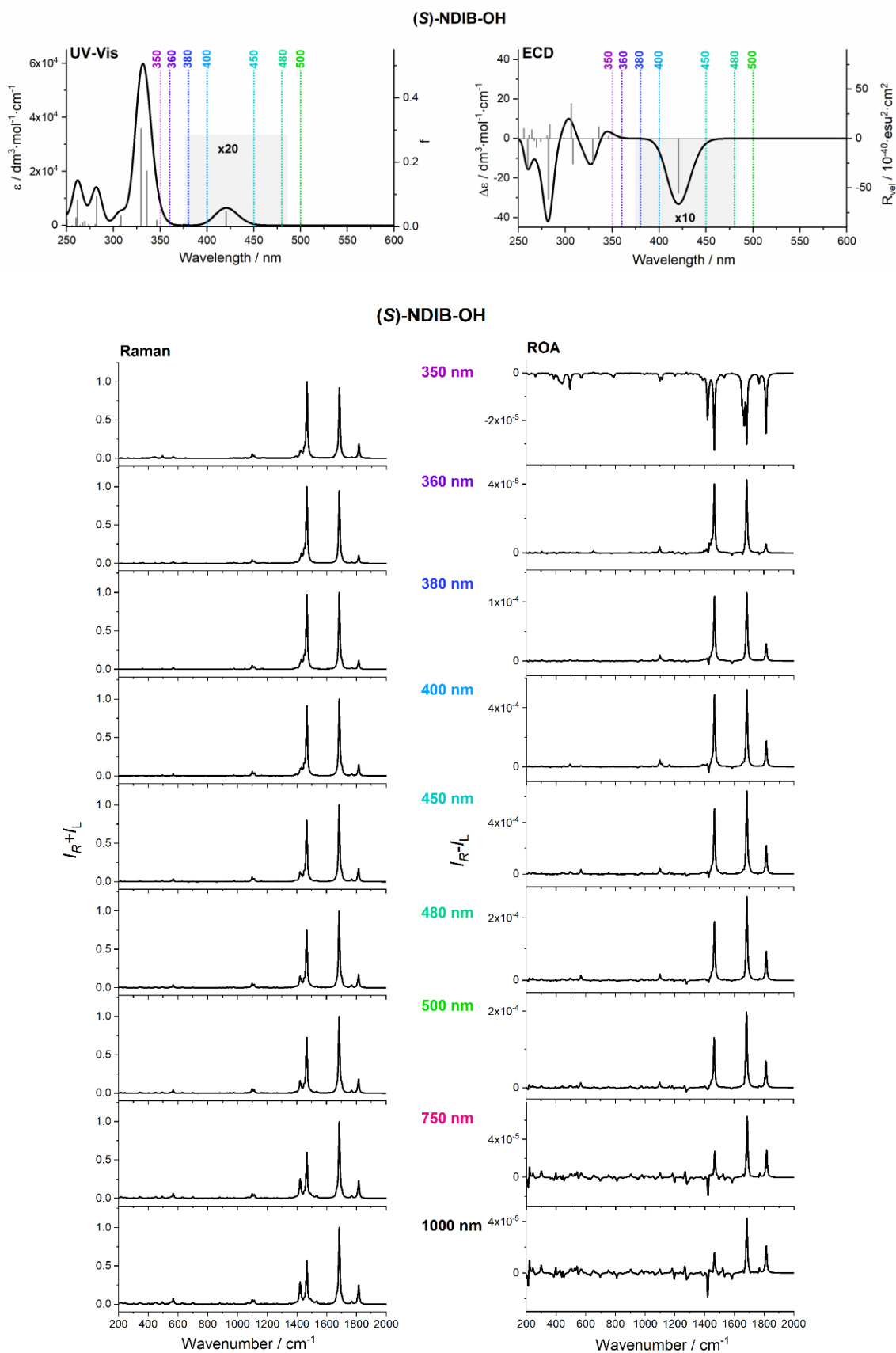
**Figure S25.** (Top) The CAM-B3LYP/ TZVP calculated UV (left) and ECD (right) spectra of (S)-NDIB-NH<sub>2</sub>. (bottom) The CAM-B3LYP/ TZVP calculated Raman (left) and ROA (right) spectra of NDIB-NH<sub>2</sub> by using different excitation lines. The ROA intensities are normalized to the Raman ones. Calculations were performed by using Gaussian 16 suit of programs.



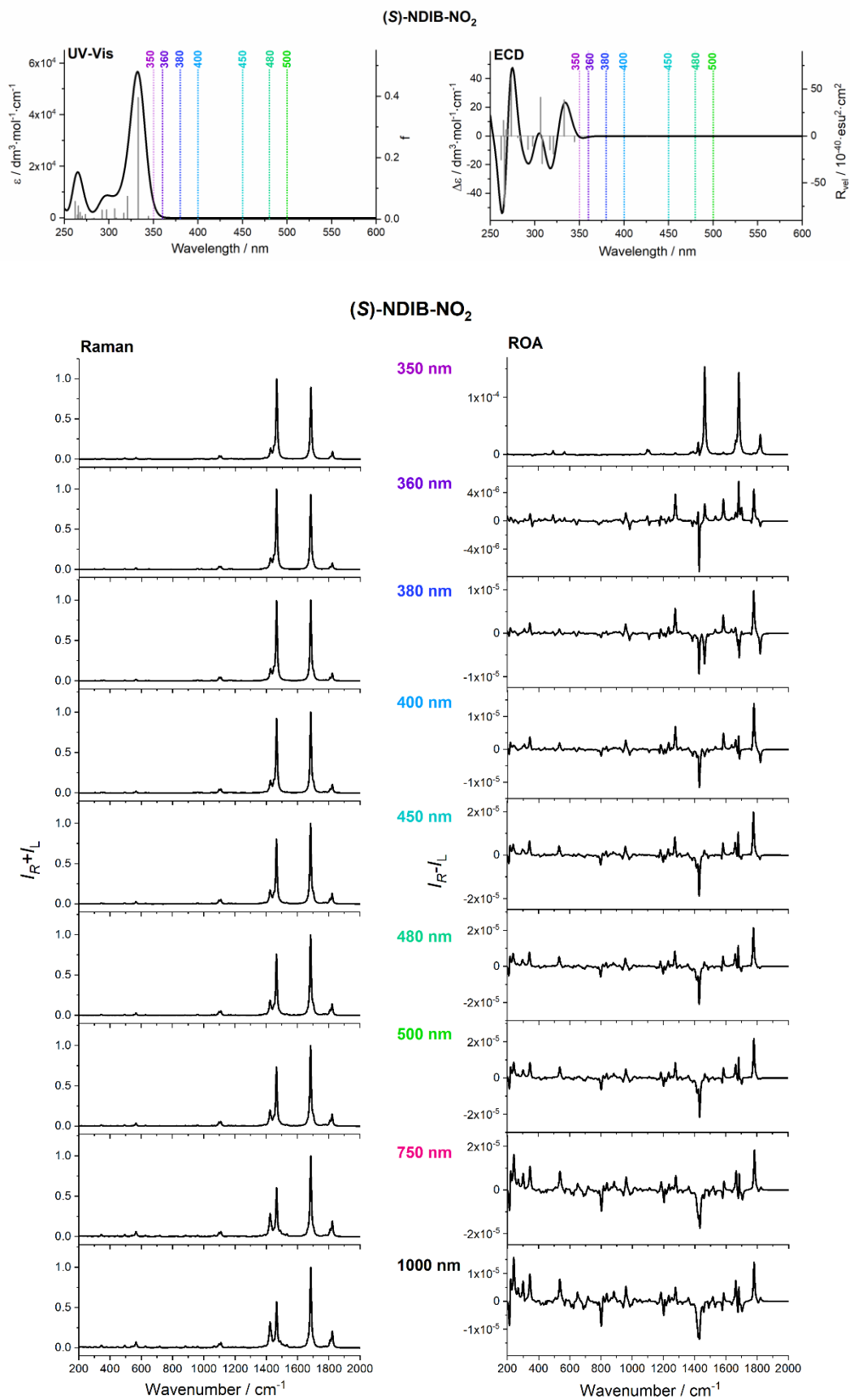
**Figure S26.** (Top) The CAM-B3LYP/ TZVP calculated UV (left) and ECD (right) spectra of (S)-NDIB-NHCH<sub>3</sub>. (bottom) The CAM-B3LYP/ TZVP calculated Raman (left) and ROA (right) spectra of NDIB-NHCH<sub>3</sub> by using different excitation lines. The ROA intensities are normalized to the Raman ones. Calculations were performed by using Gaussian 16 suit of programs.



**Figure S27.** (Top) The CAM-B3LYP/ TZVP calculated UV (left) and ECD (right) spectra of (S)-NDIB-OCH<sub>3</sub>. (bottom) The CAM-B3LYP/ TZVP calculated Raman (left) and ROA (right) spectra of NDIB-OCH<sub>3</sub> by using different excitation lines. The ROA intensities are normalized to the Raman ones. Calculations were performed by using Gaussian 16 suit of programs.



**Figure S28.** (Top) The CAM-B3LYP/ TZVP calculated UV (left) and ECD (right) spectra of (S)-NDIB-OH. (bottom) The CAM-B3LYP/ TZVP calculated Raman (left) and ROA (right) spectra of NDIB-OH by using different excitation lines. The ROA intensities are normalized to the Raman ones. Calculations were performed by using Gaussian 16 suit of programs.



**Figure S29.** (Top) The CAM-B3LYP/ TZVP calculated UV (left) and ECD (right) spectra of (S)-NDIB-NO<sub>2</sub>. (bottom) The CAM-B3LYP/ TZVP calculated Raman (left) and ROA (right) spectra of NDIB-NO<sub>2</sub> by using different excitation lines. The ROA intensities are normalized to the Raman ones. Calculations were performed by using Gaussian 16 suit of programs.

## References

- (1) Machalska, E.; Zajac, G.; Baranska, M.; Kaczorek, D.; Kawęcki, R.; Lipiński, P. F. J.; Rode, J. E.; Dobrowolski, J. Cz., *Chem. Sci.* **2021**, *12* (3), 911–916.
- (2) Guyon, M.C.; Duclos, M.C; Métay, E.; Lemaire, M., *Tetrahedron Lett.* **2016**, *57*, 3002–3005.
- (3) Sheldrick, G.M., *Acta Crystallogr. C* **2015**, *71*.
- (4) Dolomanov, O.V; Bourhis, L.J.; Gildea, R.J.; Howard, J.A.K.; Puschmann, H., *J. Appl. Crystallogr.* **2009**, *42* (2), 339–341.
- (5) Yanai, T.; Tew, D.P.; Handy, N.C., *Chem. Phys. Lett.* **2004**, *393* (1–3), 51–57.
- (6) Grimme, S.; Antony, J.; Ehrlich, S.; Krieg, H., *J. Chem. Phys.* **2010**, *132* (15).
- (7) Schäfer, A.; Horn, H.; Ahlrichs, R., *J. Chem. Phys.* **1992**, *97* (4), 2571–2577.
- (8) Schäfer, A.; Huber, C.; Ahlrichs, R., *J. Chem. Phys.* **1994**, *100* (8), 5829–5835.
- (9) Weigend, F.; Ahlrichs, R., *Phys. Chem. Chem. Phys.* **2005**, *7* (18), 3297–3305.
- (10) Weigend, F., *Phys. Chem. Chem. Phys.* **2006**, *8* (9), 1057–1065.
- (11) M. J. Frisch, G. W. Trucks, H. B. Schlegel, G. E. Scuseria, M. A. Robb, J. R. Cheeseman, G. Scalmani, V. Barone, B. Men-  
nucci, G. A. Petersson, H. Nakatsuji, M. Caricato, X. Li, H. P. Hratchian, A. F. Izmaylov, J. Bloino, G. Zheng, J. L. Sonnen-  
berg, M. Hada, M. Ehara, K. Toyota, R. Fukuda, J. Hasegawa, M. Ishida, T. Nakajima, Y. Honda, O. Kitao, H. Nakai, T.  
Vreven, J. A. Montgomery, Jr, J. E. Peralta, F. Ogliaro, M. Bearpark, J. J. Heyd, E. Brothers, K. N. Kudin, V. N. Staroverov,  
T. Keith, R. Kobayashi, J. Normand, K. Raghavachari, A. Rendell, J. C. Burant, S. S. Iyengar, J. Tomasi, M. Cossi, N. Rega,  
J. M. Millam, M. Klene, J. E. Knox, J. B. Cross, V. Bakken, C. Adamo, J. Jaramillo, R. Gomperts, R. E. Stratmann, O.  
Yazyev, A. J. Austin, R. Cammi, C. Pomelli, J. W. Ochterski, R. L. Martin, K. Morokuma, V. G. Zakrzewski, G. A. Voth, P.  
Salvador, J. J. Dannenberg, S. Dapprich, A. D. Daniels, O. Farkas, J. B. Foresman, J. V. Ortiz, J. Cioslowski and D. J. Fox,  
Gaussian 09, Re-vision D.01, Gaussian, Inc, Wallingford CT, US, **2010**.
- (12) R.D. Dennington II, T.A. Keith and J.E. Millam, GaussView 6.0.16, Semichem Inc. 2000-2016.
- (13) Ozimiński, W.P.; Dobrowolski, J.Cz., *J. Phys. Org. Chem.* **2009**, *22* (8), 769–778.
- (14) Dobrowolski, J.Cz.; Lipiński, P.F.J.; Karpińska, G., *J. Phys. Chem. A* **2018**, *122* (19), 4609–4621.
- (15) Machalska, E.; Zajac, G.; Wierzbza, A.J.; Kapitán, J.; Andruniów, T.; Spiegel, M.; Gryko, D.; Bouř, P.; Baranska, M.,  
*Angew. Chem. Int. Ed.* **2021**, *60* (39), 21205–21210.
- (16) Gaussian 16, Revision C.01, M. J. Frisch, G. W. Trucks, H. B. Schlegel, G. E. Scuseria, M. A. Robb, J. R. Cheeseman, G.  
Scalmani, V. Barone, G. A. Petersson, H. Nakatsuji, X. Li, M. Caricato, A. V. Marenich, J. Bloino, B. G. Janesko, R. Gom-  
perts, B. Mennucci, H.P. Hratchian, J. V. Ortiz, A.F. Izmaylov, J. L. Sonnenberg, D. Williams-Young, F. Ding, F. Lipparini,  
F. Egidi, J. Goings, B. Peng, A. Petrone, T. Henderson, D. Ranasinghe, V. G. Zakrzewski, J. Gao, N. Rega, G. Zheng, W.  
Liang, M. Hada, M. Ehara, K. Toyota, R. Fukuda, J. Hasegawa, M. Ishida, T. Nakajima, Y. Honda, O. Kitao, H. Nakai, T.  
Vreven, K. Throssell, J. A. Montgomery, Jr., J. E. Peralta, F. Ogliaro, M. J. Bearpark, J. J. Heyd, E. N. Brothers, K. N.  
Kudin, V. N. Sta-  
roverov, T. A. Keith, R. Kobayashi, J. Normand, K. Raghavachari, A. P. Rendell, J. C. Burant, S. S.  
Iyengar, J. Tomasi, M. Cossi, J. M. Millam, M. Klene, C. Adamo, R. Cammi, J. W. Ochterski, R. L. Martin, K. Morokuma,  
O. Farkas, J. B. Foresman, and D. J. Fox, Gaussian, Inc., Wallingford CT, **2016**.